Cooper, A.K., O'Brien, P.E., and Richter, C. (Eds.)
Proceedings of the Ocean Drilling Program, Scientific Results Volume 188

7. Data Report: Spectral Data from Sites 1165 and 1167 Including the HiRISC Section from Hole 1165B[1]

John E. Damuth[2] and William L. Balsam[2]

ABSTRACT

We measured and analyzed near-ultraviolet/visible/near-infrared spectral data from core samples recovered from Ocean Drilling Program Sites 1165 (Wild Drift) and 1167 (Prydz Channel Trough Mouth Fan) using our laboratory-grade spectrophotometer to help determine temporal mineralogical changes downhole. These measurements included closely spaced (~10 cm) samples for the section from 0 to 54.17 meters below seafloor (mbsf) in Hole 1165B, which is the Pliocene–Pleistocene age interval being studied in detail by the High-Resolution Integrated Stratigraphy Committee (HiRISC). We also determined calcium carbonate content for all samples in this HiRISC interval. The Pleistocene and uppermost Pliocene sediments (0–10 mbsf) show wide carbonate fluctuations ranging from 0 to 37 wt%; however, below 10 mbsf, the carbonate content is generally zero. To examine the major components that contribute to spectral variability in the holes, the first-derivative values for all samples from Sites 1165 and 1167 were assembled into a single matrix and the matrix was then factor analyzed after being subject to a varimax rotation. For Sites 1165 and 1167, factoring first-derivative values from 255 to 745 nm produced the most easily interpretable results, with five factors that explain ~92.5% of the total variance in the data set.

Factor 1 incorporates both goethite and chlorite, meaning that scores for this factor will be high where these two minerals covary.

[1]Damuth, J.E., and Balsam, W.L., 2003. Data report: Spectral data from Sites 1165 and 1167 including the HiRISC section from Hole 1165B. *In* Cooper, A.K., O'Brien, P.E., and Richter, C. (Eds.), *Proc. ODP, Sci. Results,* 188, 1–49 [Online]. Available from World Wide Web: <http://www-odp.tamu.edu/publications/188_SR/VOLUME/CHAPTERS/003.PDF>. [Cited YYYY-MM-DD]
[2]Department of Geology, University of Texas at Arlington, PO Box 19049, Arlington TX 76019, USA. Correspondence author: **damuth@uta.edu**

Initial receipt: 10 July 2002
Acceptance: 10 June 2003
Web publication: 17 September 2003
Ms 188SR-003

Factor 2 is interpreted as organic matter.
Factor 3 appears to be a combination of clay minerals, possibly montmorillonite and illite.
Factor 4 is interpreted as the mineral maghemite, a polymorph of hematite.
Factor 5 is the mineral hematite.

We generated plots of factor scores downhole at Sites 1165 and 1167 to determine trends in temporal changes. At Site 1165 Factor 1 predominates above ~540 mbsf, Factor 2 is important above ~280 mbsf, and Factor 3 is high from 25 to 350 mbsf. Factor 4 exhibits two zones of high values from 20 to 50 mbsf and 540 to 750 mbsf. Factor 5 is important from 0 to 95 mbsf. In the HiRISC Section of Hole 1165B (0–54 mbsf), Factors 1 and 2 exhibit high scores through most of the section, with the exception of a low in both factors centered at ~30 mbsf. Factors 3 and 4 exhibit high values primarily below 30 mbsf, and Factor 5 exhibits higher-frequency variation than the other factors. Despite apparent similarities in their downhole patterns, few of the factors are highly correlated to each other. In Hole 1167A Factor 1 is important only in the top 5 mbsf, whereas Factor 2 is important throughout the entire hole. Factor 3 is important only from 210 to 227 mbsf, Factor 4 exhibits a few high values in the uppermost 30 mbsf, and Factor 5 is most important from 30 to 210 mbsf. Regression of factor scores vs. X-ray diffraction percentage values for the various minerals downhole indicates minor correlations of Factor 1 to pyrite and Factor 2 to hornblende. No other factors exhibited a correlation >0.1 for any of the minerals analyzed.

INTRODUCTION AND BACKGROUND

Marine geologists have used color, which is the human eye's perception of reflected radiation in the visible region of the electromagnetic spectrum (400–700 nm), to describe marine sediment cores for many years. Sediment color is usually determined visually by comparison to a color chart like the Geological Society of America Rock Color Chart (Goddard et al., 1948), which is a derivative of the Munsell Color Chart. Such color-chart analysis is qualitative and inexact because no two observers have the same color perception. Color also tends to obscure differences in visible spectra because similar colors may result from the mixing of different spectral wavelengths, a condition termed *metamerism*. Many of the problems related to qualitative color analysis can be overcome by using diffuse-reflectance spectrophotometry, a technique in which light reflected from a sample is collected in a reflectance sphere and compared to light reflected from a pure white standard throughout the wavelength range being analyzed. The quantitative data produced by this technique are reflectance values as a function of wavelength relative to the standard.

Attempts to use reflectance spectra without respect to color to interpret marine cores dates back to the mid-1960s (e.g., Chester and Elderfield, 1966, 1968; Chester and Green, 1968); however, a concerted effort to exploit near-ultraviolet (NUV), visible (VIS), and near-infrared (NIR) spectral reflectance as a marine geological research tool has only recently been undertaken. Deaton (1987) quantified Munsell color-chart chips with a reflectance spectrophotometer in an attempt to help geologists relate color to spectra. Although such analysis of color chips makes the determination of color more precise, it does not alleviate the prob-

lems associated with the scientific use of color. Studies by Barranco et al. (1989), Deaton and Balsam (1991), Balsam and Deaton (1991, 1996), Balsam et al. (1998), Herbert et al. (1992), and Mix et al. (1992) have shown that many marine sediment components have distinctive spectral signatures. VIS reflectance spectra have been used to identify the iron oxide and oxyhydroxide minerals hematite and goethite; the clay minerals illite, montmorillonite, and chlorite; calcite; and sediment organic content (Deaton and Balsam, 1991; Balsam and Deaton, 1991; Balsam et al., 1998). Balsam and Deaton (1996) obtained quantitative estimates of carbonate, opal, and organic content by applying regression techniques to NUV/VIS/NIR spectra.

Herbert et al. (1992) used infrared reflectance spectra from a Fourier transform infrared spectrophotometer (FTIR) to quantify the abundances of a number of minerals including calcite, quartz, and various clay minerals. Both the reflectance spectrophotometer used by Balsam and Deaton and the FTIR used by Herbert et al. analyze only one sample at a time, and each sample has to be changed manually. Both machines take ~60 s to analyze a sample; the FTIR actually performs a single analysis in 5 s but uses numerous stacked analyses to remove noise. Mix et al. (1992, 1995) developed a VIS/NIR scanning spectrophotometer that can be deployed at sea. This instrument has been utilized to scan cores aboard the *JOIDES Resolution* and is capable of analyzing a small area of a core's surface (about a 2-cm circle) in 5 s, then automatically advancing down the core and making subsequent measurements. More recently, compact handheld spectrophotometers, such as the Minolta CM-2002, have become available and are being routinely used to measure color spectra of sediments in the laboratory and at sea without having to take and prepare sediment samples. A Minolta CM-2002 instrument has been routinely used during the past 10 yr during core description and processing during Ocean Drilling Program (ODP) legs aboard the *JOIDES Resolution*, and the data are commonly used to correlate from core to core, to determine glacial–interglacial climatic cycles, and to determine mineral compositions downcore (e.g., Mix et al., 1992, 1995; Schneider et al., 1995; Balsam et al., 1997, 1998, 1999; Balsam and Damuth 2000; Giosan et al., 2001).

In a series of previous studies based on cores from ODP legs and existing piston cores, we (W. Balsam and J. Damuth) have compared the results of spectral data collected at sea on board the *JOIDES Resolution* with the handheld Minolta CM-2002 spectrophotometer and our shore-based, research-grade spectrophotometer (PerkinElmer Lambda 6) (Balsam et al., 1997, 1998, 1999; Balsam and Damuth, 2000). Comparison of spectra from wet cores measured aboard ship with the Minolta instrument to spectra measured from comparable core samples using a shore-based PerkinElmer Lambda 6 spectrophotometer showed that although the spectral signal is muted in the percent reflectance curves from the wet shipboard sediments compared to curves generated from dry core samples onshore, both sets of reflectance curves are quite similar when processed using a first-derivative transformation. This observation is further supported by factor analysis of parallel (shipboard vs. shore based) data sets (400-700 nm) produced by the two instruments (Balsam et al., 1997; Balsam and Damuth, 2000).

Data Collection and Sample Interval for the Present Study

For the present report we measured and analyzed spectral data from core samples recovered at ODP Sites 1165 and 1167 using our laboratory-grade PerkinElmer Lambda 6 spectrophotometer, referred to above. Site 1165 is from the Wild Drift, a large contourite drift deposit on the continental rise seaward of Prydz Bay, and Site 1167 is from the Prydz Channel Trough Mouth Fan on the continental slope seaward of Prydz Channel (O'Brien, Cooper, Richter, et al., 2001). We did not analyze any cores from Site 1166 on the continental shelf because of the sparse core recovery and the lithified and disturbed nature of much of the recovered sediments.

At Site 1165, Wild Drift, we determined NUV/VIS/NIR spectra for closely spaced (~10 cm) samples for the interval from Sections 188-1165B-1H-1, 0 cm, through 6H-7, 38 cm (0–54.17 meters below seafloor [mbsf]), in Hole 1165B, which is the Pliocene–Pleistocene age interval being studied in detail by the High-Resolution Integrated Stratigraphy Committee (HiRISC) and described in this volume (e.g., **Warnke et al.,** this volume). We also determined calcium carbonate content for all samples in this HiRISC interval. Sample spacing for NUV/VIS/NIR spectral studies below 54 mbsf for holes 1165B and 1165C, as well as throughout Hole 1167A from the Prydz Channel Trough Mouth Fan, was on the order of one sample per core section (i.e., 1–2 m spacing). We did not routinely determine calcium carbonate downhole below 54 mbsf at Site 1165 or for any interval at Site 1167 because spot checks suggested that the carbonate content was at or near zero throughout these sections. Table **T1** lists all samples used for this study. The carbonate and spectrophotometer analyses were conducted at the University of Texas at Arlington (UTA).

T1. Calcium carbonate, brightness, reflectance, and factor scores, p. 47.

CALCIUM CARBONATE CONTENT IN THE HIRISC SECTION, HOLE 1165B

We used the vacuum-gasometric technique of Jones and Kaiteris (1983) to determine weight percent calcium carbonate content for all samples downhole in Hole 1165B from 0 to 54 mbsf (Fig. **F1;** Table **T1**). With this technique a small (~0.25 g) pulverized sample is digested in concentrated phosphoric acid under vacuum, and the pressure generated by the release of CO_2 is recorded on a vacuum gauge. Weight percent $CaCO_3$ is calculated by relating the pressure increase in the sample to the pressure increase in reagent carbonate after correcting for temperature and pressure. The Jones and Kaiteris (1983) technique has an accuracy of about ±1%. As with most techniques used to determine percent carbonate, the Jones and Kaiteris (1983) technique lumps together both polymorphs of $CaCO_3$, calcite, and aragonite, as well as carbonate from biogenic and nonbiogenic sources. In most marine settings dolomite is not a significant contributor to the carbonate component.

This interval from 0 to 54 mbsf is the HiRISC Pliocene–Pleistocene section that extends back to ~5 Ma (**Warnke et al.,** this volume). We ran samples spaced at ~10-cm intervals down this section (Fig. **F1;** Table **T1**). The sample locations were chosen by the High-Resolution Integrated Stratigraphy Committee. The Pleistocene and uppermost Pliocene sediments in this section (0–10 mbsf) show wide fluctuations

F1. Calcium carbonate and brightness, HiRISC, p. 17.

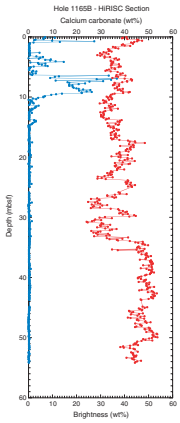

in carbonate content ranging from 0 to 37 wt% (Fig. F1). Below 10 mbsf the carbonate content is generally zero and rarely rises to a few weight percent. In Table T1 most of the values in this interval are <0.4 wt%, values that are below the accuracy of the instrument.

NUV/VIS/NIR SPECTRAL ANALYSIS OF SEDIMENTS

Data Preparation and Analysis

NUV/VIS/NIR spectral data were measured from all samples taken from Sites 1165 and 1167 with our laboratory-grade PerkinElmer Lambda 6 spectrophotometer at UTA (see the "Appendix," p. 16, for raw data). Sample preparation followed the procedures described by Balsam and Deaton (1991). Each sample was ground to <38 µm, made into a thick slurry on a glass microslide with distilled water, and slowly dried either in air or on the lowest setting of a hot plate. Reflectance spectrophotometers such as ours are designed to scan different wavelengths of light reflected from a sample's surface and record the intensity of that reflected light relative to a white standard (e.g., barium sulfate) used to set the 100% reflectance level. The PerkinElmer Lambda 6 spectrophotometer we use is equipped with a reflectance sphere, which is a diffuse reflectance attachment that allows total reflectance measurements to be made. The Lambda 6 contains two light sources (a tungsten lamp for 350–850 nm and a deuterium lamp for 250–350 nm), a moving grating (to separate light into different wavelengths), and a photomultiplier tube (to measure the intensity of light reflected from the sample surface). Data from the spectrophotometer are recorded directly on a floppy disk at 1-nm intervals from 250 to 850 nm, the analytical range of the Lambda 6 in reflectance mode. Samples were analyzed using a slit width of 2 nm and were scanned at 600 nm/min. The actual time per analysis, including changing samples, is 2–3 min. The percent reflectance measured for each sample at 10-nm intervals is presented in the "Appendix," p. 16. These data were used to determine the brightness, reflectance of specific color bands (e.g., red, green, etc.), and factor scores given in Table T1 and described below. In Table T1 the brightness, percent brightness, and percent reflectance for six specific color bands were calculated only from samples in the VIS range (400–700 nm); whereas the factor scores identified through factor analysis of the data were calculated using sample data from the entire spectral range (250–850 nm). In the accompanying figures, we display curves showing brightness downhole as *percent brightness*, which is simply brightness values rescaled to 100%.

Sediment Brightness Determined from Spectral Data

HiRISC Section

Sediment brightness (sometime termed lightness) is calculated as the area under the spectral curve in the VIS (400–700 nm) portion of the spectrum. Brightness measured in marine sediments commonly shows a positive correlation with calcium carbonate, especially in pelagic sediments, and thus is sometimes used as a proxy for carbonate content; however, other factors can also influence brightness (see Balsam et al., 1999, for detailed discussion). Figures F1 and F2 show the brightness for

F2. Brightness, HiRISC, p. 18.

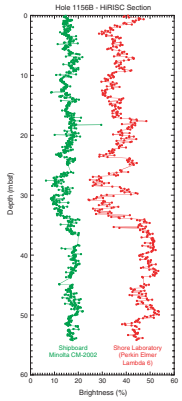

the HiRISC section (0–54 mbsf) in Hole 1165B. Figure F3 shows percent reflectance curves for six color bands (Table T1). Note that in the upper 10 m of the section, the brightness does seem to correlate with the carbonate content. However, for the remainder of the section, where carbonate is essentially zero, the brightness also varies widely and, thus, must be related to mineralogical components other than carbonate. For example, the brightness curve seems to correlate quite well with magnetic parameters, bulk density, and natural gamma radiation curves from the HiRISC section (see Warnke et al., this volume). In particular, a major change in sediment properties at the beginning of the late Pliocene recorded in these parameters is clearly recorded by an overall sharp decrease in brightness at ~34 mbsf (Fig. F2).

The brightness for the HiRISC section derived from shipboard measurements using the Minolta CM-2002 spectrophotometer is also shown in Figure F2. During Leg 188 the Minolta instrument was mounted on the archive multisensor track (see O'Brien, Cooper, Richter, et al., 2001, for details), and all spectral measurements were automated and performed on the archive half of each core. Because of this automated process, erroneous measurements were commonly made at gaps, voids, and missing intervals of core because of coring disturbance or gas expansion. Other erroneous measurements were made on rock clasts and at locations where the sensor was not able to align itself flush against the core surface so that light escape was minimal. The shipboard sedimentologists carefully recorded the intervals with these erroneous measurements for each section measured. The Minolta data shown in Figure F2 is an edited subset of the original shipboard data set in which all of these erroneous measurements have been deleted, as far as possible (Table T2). Note that the shipboard brightness data fluctuations correlate quite well with the PerkinElmer–derived data, except that the brightness for the sediments measured with the Minolta is consistently lower than those values measured with the PerkinElmer. We have conducted several studies on cores from previous ODP legs comparing shipboard Minolta measurements, which by necessity must be conducted on wet cores, with PerkinElmer measurements, which must be made on dry ground-up core sediments (Balsam et al., 1997, 1998, 1999; Balsam and Damuth, 2000). These studies showed that water in the sediments mutes the brightness; however, when both sets of reflectance curves are processed using a first-derivative transformation, the shipboard and shore-based analyses are quite similar and suggest that accurate, reliable spectral data can be obtained from wet cores at sea using the Minolta spectrophotometer. We did not conduct any additional comparative studies between the Minolta and PerkinElmer data sets from Leg 188 sediments because we are satisfied that our previous studies (cited above) have adequately resolved this question and that any such comparison (e.g., data in Fig. F2) would yield similar results.

Sites 1165 and 1167

Figure F4 shows the brightness down Holes 1165B and 1165C from the Wild Drift. The brightness is highly variable in the top 300 mbsf of Hole 1165B. This variability reflects the cyclicity in sedimentation since the middle Miocene with sediments containing numerous alternations or cycles between biogenic material and clay-sized terrigenous detritus (Shipboard Scientific Party, 2001). Detailed analysis of two short (~15 m) intervals within these cyclic sediments by the Shipboard Scientific

F3. Reflectance, HiRISC, p. 19.

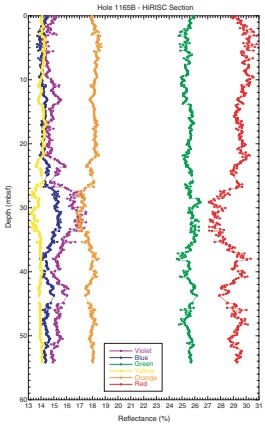

T2. Brightness from shipboard and shore-based analyses, p. 48.

F4. Brightness, Site 1165, p. 20.

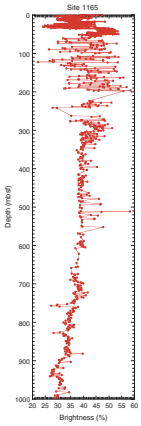

Party (2001) showed that this cyclicity appears to occur with Milankovitch periodicities. Below 300 mbsf the sediments show less variation in brightness and brightness decreases slightly downhole (Fig. F4). The sediments below 400 mbsf are dark greenish gray clays with numerous thin silt laminae and represent classic contourites contained in the Wild Drift (O'Brien, Cooper, Richter, et al., 2001). Figure F5 shows percent reflectance of six discrete color bands down Site 1165.

Figure F6 shows the brightness down Hole 1167A from the Prydz Channel Trough Mouth Fan. The brightness is generally low down the entire hole because the sediments are uniformly dark gray to dark greenish gray silty sandy clays and clayey silts and sands with numerous rock clasts and pebbles (O'Brien, Cooper, Richter, et al., 2001). There are also numerous gaps in core recovery, which make recognition of downhole trends in brightness difficult to recognize, if present. The spike in increased brightness at the top of the hole is due to a thin layer of hemipelagic sediment that overlies the thick section of debris flows beneath. Figure F7 shows percent reflectance of six color bands down Hole 1167A.

F5. Reflectance, Site 1165, p. 21.

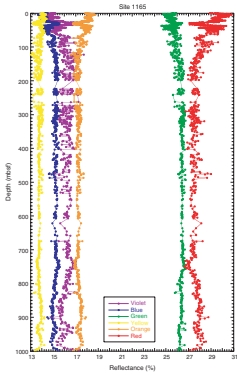

F6. Brightness, Hole 1167A, p. 22.

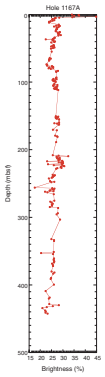

F7. Reflectance, Hole 1167A, p. 23.

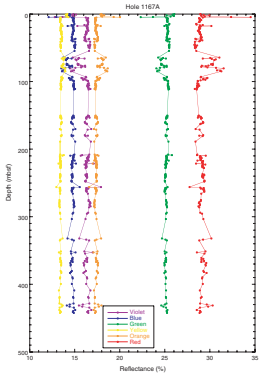

F8. First-derivative curve identifies diagnostic mineral peaks, p. 24.

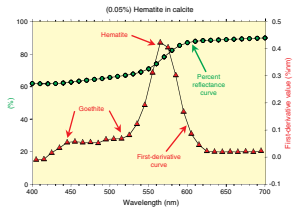

IDENTIFICATION OF SEDIMENT COMPONENTS AND MINERALS WITH DIFFUSE REFLECTANCE SPECTROPHOTOMETRY USING FACTOR ANALYSIS

First-Derivative Values

NUV/VIS/NIR percent reflectance spectra from marine cores are relatively featureless and exhibit few of the diagnostic absorption features that are typically used to identify materials by their spectrum (Barranco et al., 1989). The variability of percent reflectance spectra may be enhanced by taking the first derivative (percent reflectance per nanometer) at specific wavelength intervals (Fig. F8). First-derivative values are high where the slope of the percent reflectance curve changes rapidly. We calculated first-derivative values for each sample at 10-nm intervals from 250 to 850 nm (resulting in 60 first-derivative values per sample) (see the "Appendix," p. 16). Each value was then plotted at the midpoint of each 10-nm interval (i.e., the 400- to 410-nm first-derivative value is plotted at 405 nm, etc.). Typically, first-derivative curves reveal more peaks than untransformed percent reflectance curves (Fig. F8) (also see Barranco et al., 1989, and Balsam and Deaton, 1991, for examples). These peaks are characteristic of different minerals and sediment components (Balsam and Deaton, 1991; Balsam and Damuth, 2000). The first-derivative transformation also de-emphasizes the importance of absolute percent reflectance values, thereby reducing the significance of slight differences in calibration, sample thickness, and sample orientation.

Factor Analysis

To examine the major components that contribute to spectral variability, the first-derivative values for all the samples from Sites 1165 and 1167 were assembled into a single matrix (samples = rows; first-derivative values for wavelengths = columns) and the matrix factor analyzed after being subject to a varimax rotation. Factor analysis was performed

with SysStat (version 7.0.1), a product of SPSS Inc. Factor analysis of the first derivative values produces factors that group covarying first-derivative wavelengths. For Sites 1165 and 1167, factoring first-derivative values from 255 to 745 nm produced the most easily interpretable results, with five factors (described below) that explain ~92.5% of the total variance in the data set. Each of these factors explain at least 5% of the variance in the data set; for these five factors, the variance explained by each factor after rotation from Factor 1 to Factor 5 is 34.1%, 34.0%, 12.7%, 5.9%, and 6.0%.

The primary method used to interpret factors in this study is factor description diagrams, which are plots of the importance of each wavelength (i.e., factor loading) through the wavelength range analyzed (factor pattern curve) (Fig. F9). The resulting factor description curve is then compared to first-derivative curves for known minerals, combinations of minerals and sediment components (e.g., hematite in Fig. F9). Balsam and Deaton (1991) demonstrated that this method can be used to identity iron oxide and clay mineral factors in modern Atlantic Ocean sediments. For Sites 1165 and 1167, all the factor description curves can be related to first-derivative curves for known minerals or sediment components (Figs. F10–F14).

F9. Interpretation of a factor curve, p. 25.

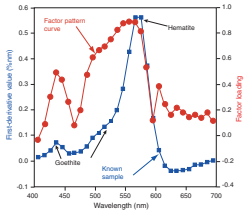

However, factor analysis adds a complication to the interpretation of diffuse reflectance spectrophotometer (DRS) data. Factors are assemblages of variables that exhibit similar patterns, that is, covariance. If two minerals or substances are always found together, they will occur in the same factor. As a result of differing spectral strengths, the dominant spectral signal in a factor may not be the component with the highest weight concentration. Nevertheless, we name factors after the dominant spectral component. In addition, some common minerals with a weak spectral signal, for example, illite, may be completely masked by other minerals with stronger spectral signals. For such a case, it is unlikely illite would contribute to a factor, even if it constituted a substantial proportion of the sediment.

For downhole data from Sites 1165 and 1167, factor interpretation may be aided by plotting their distribution downhole using factor scores, which indicate how important each factor is in each sample (e.g., Figs. F15–F29). Ideally, these downhole plots are then compared to downhole distributions of various sediment components identified by other means (e.g., X-ray diffraction [XRD]). There are some important similarities and differences between reflectance data and data generated by other commonly used analytical techniques such as XRD. In several ways, reflectance data derived from DRS are similar to those derived from XRD. First-derivative peak height, like the height of XRD peaks, is a function of both the concentration of a substance (mineral for XRD) and the composition of the matrix in which it is found (Deaton and Balsam, 1991; Balsam et al., 1999). DRS data differ from XRD in three important respects. First, DRS is not limited to crystalline material; spectra can be obtained from any substance. Second, the heights of first-derivative peaks are not only a function of mineral concentration and matrix material but also are a function of the "spectral strength" of a substance. Some substances (e.g., hematite) have a persistent spectral signal that is capable of concealing the peaks of other substances. Third, for some substances, the DRS limits of resolution differ significantly from those of XRD. For example, depending on the matrix, hematite can be detected at a concentration of ~0.01% by weight with DRS, whereas with XRD, the limit of resolution without special sample prep-

aration is ~1% (Deaton and Balsam, 1991). To date, limits of resolution with DRS have been determined for only a very few minerals, sediment components, and combinations of components. For XRD, a similar statement applies for many minerals and mineral combinations.

Finally, it is important to remember that DRS is not color analysis. Color is the human eye's perception of reflected wavelengths in the visible region of the electromagnetic spectrum. Color can be derived from the VIS spectrum, but because of the way the human eye mixes wavelengths, color is not the same as VIS spectral analysis. For example, the eye perceives brown and purple as colors; however, these are not spectral colors but colors that result from the eye's method of signal processing. The spectrophotometer is not only far more discriminating than the human eye in assessing the VIS spectrum but also has a lower detection limit. Therefore, features identified with the spectrophotometer may not be visible to the naked eye.

Interpretation of Factors

As stated above, we identify five factors from the sediments at Sites 1165 and 1167, and we interpret these factors as follows.

Factor 1

We interpret Factor 1 as incorporating both goethite and chlorite, meaning that scores for this factor will be high where these two minerals covary. The peak at 315 nm is indicative of the chlorite mineral ripidolite, whereas the peaks at 445 and 525 nm are indicative of goethite (Fig. **F10A, F10B**). The spectral curve for 1% goethite and 30% ripidolite in a matrix of 60% silica and 9% calcite bears strong resemblance to the Factor 1 curve. There are several points worth noting in this interpretation. First, the "spectral strength" of goethite is substantially greater than that of ripidolite. Even 30% ripidolite is not enough to make its signal predominate over 1% goethite where the goethite signal is strongest, that is, between ~400 and 550 nm (Fig. **F10C**). However, the ripidolite signal does affect the goethite signal in subtle ways by shifting the wavelength of peaks and influencing peak height. Second, we do not intend to imply that the chlorite mineral responsible for the 315-nm peak actually is ripidolite. There is a large variety of chlorite minerals, and we use ripidolite as a likely example. Further, for many natural materials and especially clay minerals, compositions are highly variable, resulting in changing spectral patterns. Iron oxides and oxyhydroxides, on the other hand, seem to have very consistent spectral patterns in our standards and in the natural material we have analyzed.

F10. Factor 1 curve, p. 26.

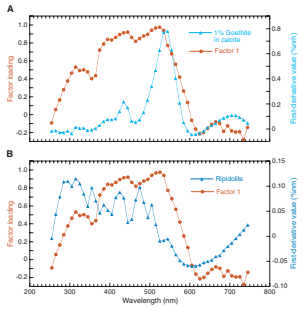

Factor 2

Factor 2 is interpreted as an organic matter factor. We compare the factor description diagram for Factor 2 to a sample containing topsoil and lignite (Fig. **F11**). Balsam and Wolhart (1993) used an identical comparison to interpret an organic factor in sediments of the Argentine Basin. They found that the mixture of topsoil and lignite provided a good sample with organic material in various stages of maturation from very immature humus in the topsoil to mature organic material in the lignite. A sample with this range of maturity is necessary because as organic matter matures it changes from a golden brown to black, resulting in an absorption band that moves across the visible portion of the

F11. Factor 2 curve, p. 28.

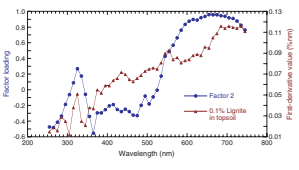

spectrum (Deaton et al., 1996). For completely mature organic matter the absorption band occupies the entire VIS, producing a black color. Like clay minerals, there is a wide variety of organic materials, each of which produce a unique spectral signal.

Factor 3

Factor 3 appears to be a combination of clay minerals, possibly montmorillonite and illite. The factor description curve exhibits major peaks at 295 and 375 nm and secondary peaks at 405, 455, 525, and 555 nm. The two major peaks are indicative of both montmorillonite (Fig. F12A) and illite (Fig. F12B), as is the low peak at 355 nm. However, the minor peaks at 405, 455, and 525 match more closely to montmorillonite than illite. Neither montmorillonite nor illite has a peak at 555 nm. Because clay minerals exhibit a variety of compositions, exact matches are unlikely; nevertheless, we consider it likely this factor represents a combination of the clay minerals illite and montmorillonite.

F12. Factor 3 curve, p. 29.

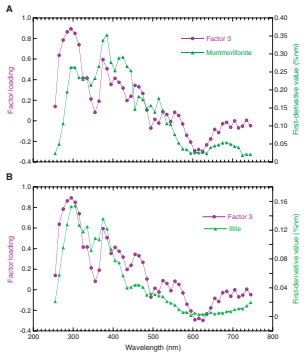

Factor 4

Factor 4 is interpreted as the mineral maghemite, a polymorph of hematite (Fig. F13). Maghemite is a well-known brown mineral that is used for the coating on floppy disks. The interpretation of this factor as maghemite is based on the coincidence of peaks, especially the location and width of the peak centered at 595 nm (Fig. F13). The factor loading peaks at 325 and 445 nm have nearby corresponding peaks in the maghemite record suggesting other minerals in the samples have offset these minor peaks. The major maghemite peak at 665 nm is not present in the factor description plot, perhaps because it is being suppressed by organic matter (Fig. F11). The presence of maghemite is surprising because it normally oxidizes to form hematite.

F13. Factor 4 curve, p. 30.

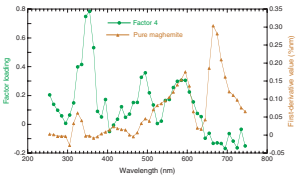

Factor 5

Factor 5 clearly contains the mineral hematite. Hematite has a first-derivative peak at 575 nm that matches a broader factor loading peak centered at this wavelength (Fig. F14). The width of the peak centered at 575 nm suggests that other minerals may be involved. We suspect that other mineral is maghemite. Maghemite not only has broad peak centered 585 nm, but also has secondary peak at 325 nm (Fig. F13), which closely overlaps the 335-nm Factor 5 loading peak. This factor may represent zones in the holes where maghemite is in the process of being oxidized to hematite.

F14. Factor 5 curve, p. 31.

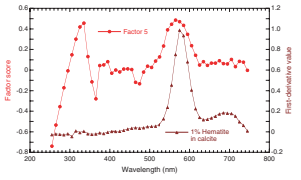

Downhole Variations in Factor Scores

Factor scores describe how important each factor is in each sample. Positive factor scores indicate that a factor is important, whereas negative scores indicate lack of importance. The larger the value of the score, the more significance (positive score) or the less significance (negative) of the factor. Plots of factor scores downhole at ODP sites indicate temporal changes in the factors. All samples from Sites 1165 and 1167 were factor analyzed as a single data set, resulting in factors that are the same for the two sites and, thus, can be compared from site to site. However, the two sites show some significant differences in the downhole distribution of factor scores.

Site 1165

At Site 1165 Factors 1, 2 and 3 are important in large segments of the hole (Figs. F15, F16, F17). Factor 1 predominates above ~540 mbsf, Factor 2 is important above ~280 mbsf, and Factor 3 is high from 25 to 350 mbsf, especially from 30 to 200 mbsf. Factor 4 exhibits two zones of high values from 20 to 50 mbsf and 540 to 750 mbsf, especially from 715 to 750 mbsf (Fig. F18). Factor 5 is important from 0 to 95 mbsf (Fig. F19). Interestingly, Factor 5 exhibits a low from 715 to 750 mbsf, whereas Factor 4 exhibits a high. However, a regression of Factor 4 vs. Factor 5 shows no statistical correlation, which suggests this inverse relationship is not a general phenomenon. Regression of the five factor scores vs. XRD percentage values for hornblende, total clay, quartz, K-feldspar, plagioclase, calcite, and pyrite downhole for Site 1165 (O'Brien, Cooper, Richter, et al., 2001) indicates minor correlations of Factors 3 and 4 to pyrite (r^2 = 0.17 for Factor 3 and r^2 = 0.12 for Factor 4). No other factors exhibited a correlation >0.1 for any of the minerals analyzed.

HiRISC Section of Hole 1165B

In the HiRISC section of Hole 1165B (0–54 mbsf), Factors 1 and 2 exhibit high scores through most of the section, with the exception of a low in both factors centered at ~30 mbsf (Figs. F20, F21). Factors 3 and 4 exhibit high values primarily below 30 mbsf (Figs. F22, F23). Factor 5 exhibits higher-frequency variation than the other factors and, with the exception of a few points, contains primarily high values below ~10 mbsf (Fig. F24). Despite apparent similarities in their downhole patterns, few of the factors are highly correlated to each other. The highest linear correlation is exhibited by Factors 2 (organic matter) and 5 (hematite) (r^2 = 0.51). This correlation is difficult to explain. The next highest linear correlation is Factors 3 (montmorillonite and illite) and 4 (maghemite) (r^2 = 0.36). One possible explanation for this correlation is that the maghemite is being transported with clay minerals or is produced by the erosion of clays. Factor 1 (goethite and ripidolite) and Factor 5 (hematite) exhibit a linear correlation (r^2 = 0.23). Hematite and goethite are end-members of oxidizing chemical processes, with hematite forming under dry and hot conditions and goethite under more humid conditions. There is substantial overlap in their formation, and both are commonly found together. The fact that this factor analysis separates hematite and goethite into two factors suggests that these minerals have different sources. Factor 3 (montmorillonite and illite) and Factor 5 (hematite) exhibit a linear correlation (r^2 = 0.21). As above, one possible explanation of this correlation is that the hematite is being transported with clay minerals or is produced by the erosion of clays. No other factors exhibit linear correlations with an $r^2 > 0.2$.

Hole 1167A

In Hole 1167A Factor 1 is important only in the top 5 mbsf (Fig. F25), Factor 2 is important throughout the entire hole (Fig. F26), Factor 3 is important only from 210 to 227 mbsf (Fig. F27), Factor 4 exhibits a few high values in the uppermost 30 mbsf (Fig. F28), and Factor 5 is most important from 30 to 210 mbsf (Fig. F29). Regression of factor scores vs. XRD percentage values for the various minerals downhole (O'Brien, Cooper, Richter, et al., 2001) indicates minor correlations of Factor 1 to

F15. Factor 1, Site 1165, p. 32.

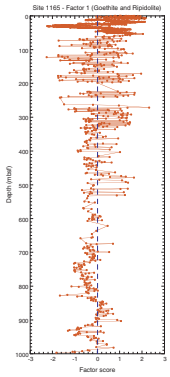

F16. Factor 2, Site 1165, p. 33.

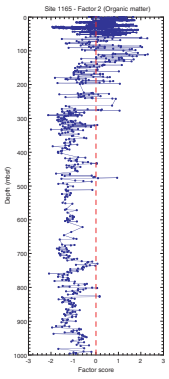

F17. Factor 3, Site 1165, p. 34.

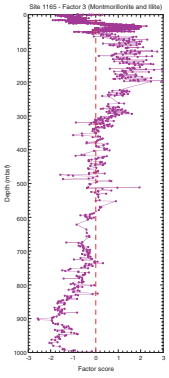

F18. Factor 4, Site 1165, p. 35.

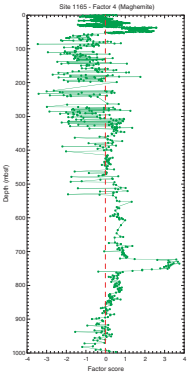

pyrite (r^2 = 0.24) and Factor 2 to hornblende (r^2 = 0.39). No other factors exhibited an $r^2 > 0.1$ for any of the minerals analyzed. It is important to note that these low correlations do not indicate a causal relationship. Rather, the factor and the mineral may show similar variations because they respond to similar conditions.

ACKNOWLEDGMENTS

This research used samples and/or data provided by the Ocean Drilling Program (ODP). ODP is sponsored by the U.S. National Science Foundation (NSF) and participating countries under management of Joint Oceanographic Institutions (JOI), Inc. J.E. Damuth was supported by USSP Grant 418928-BA356. V. Patino conducted all the spectral and carbonate measurements and was supported by the same grant. W.L. Balsam kindly contributed his time to this project at no charge.

F19. Factor 5, Site 1165, p. 36.

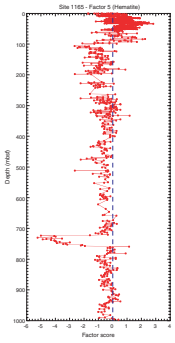

F20. Factor 1, HiRISC Hole 1165B, p. 37.

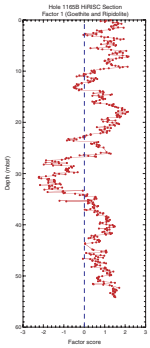

F21. Factor 2, HiRISC Hole 1165B, p. 38.

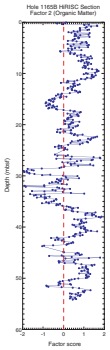

F22. Factor 3, HiRISC Hole 1165B, p. 39.

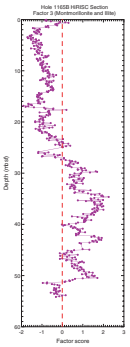

F23. Factor 4, HiRISC Hole 1165B, p. 40.

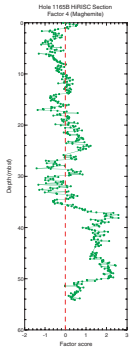

F24. Factor 5, HiRISC Hole 1165B, p. 41.

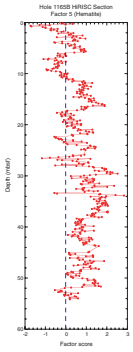

F25. Factor 1, Hole 1167A, p. 42.

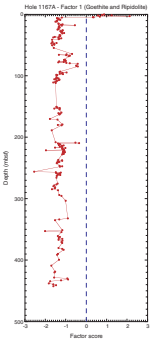

F26. Factor 2, Hole 1167A, p. 43.

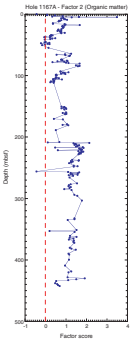

F27. Factor 3, Hole 1167A, p. 44.

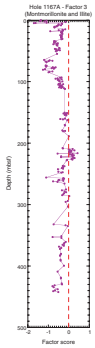

F28. Factor 4, Hole 1167A, p. 45.

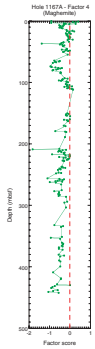

F29. Factor 5, Hole 1167A, p. 46.

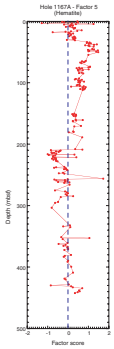

REFERENCES

Balsam, W.L., and Damuth, J.E., 2000. Further investigations of shipboard vs. shore-based spectral data: implications for interpreting Leg 164 sediment composition. *In* Paull, C.K., Matsumoto, R., Wallace, P., and Dillon, W.P. (Eds.), *Proc. ODP, Sci. Results,* 164: College Station, TX (Ocean Drilling Program), 313–324.

Balsam, W.L., Damuth, J.E., and Schneider, R.R., 1997. Comparison of shipboard vs. shore-based spectral data from Amazon-Fan cores: implications for interpreting sediment composition. *In* Flood, R.D., Piper, D.J.W., Klaus, A., and Peterson, L.C. (Eds.), *Proc. ODP, Sci. Results,* 155: College Station, TX (Ocean Drilling Program), 193–215.

Balsam, W.L., and Deaton, B.C., 1991. Sediment dispersal in the Atlantic Ocean: evaluation by visible light spectra. *Rev. Aquat. Sci.,* 4:411–447.

————, 1996. Determining the composition of late Quaternary marine sediments from NUV, VIS, and NIR diffuse reflectance spectra. *Mar. Geol.,* 134:31–55.

Balsam, W.L., Deaton, B.C., and Damuth, J.E., 1998. The effects of water content on diffuse reflectance measurements of deep-sea core samples: an example from ODP Leg 164 sediments. *Mar. Geol.,* 149:177–189.

————, 1999. Evaluating optical lightness as a proxy for carbonate content in marine sediment cores. *Mar. Geol.,* 161:141–153.

Balsam, W.L., and Wolhart, R., 1993. Sediment dispersal in the Argentine Basin: evidence from visible light spectra. *Deep-Sea Res. Part A,* 40:1001–1031.

Barranco, F.T., Jr., Balsam, W.L., and Deaton, B.C., 1989. Quantitative reassessment of brick red lutites: evidence from reflectance spectrophotometry. *Mar. Geol.,* 89:299–314.

Chester, R., and Elderfield, H., 1966. The infra-red determination of total carbonate in marine carbonate sediments. *Chem. Geol.,* 1:277–290.

————, 1968. The infra-red determination of opal in siliceous deep-sea sediments. *Geochim. Cosmochim. Acta,* 32:1128–1140.

Chester, R., and Green, R.N., 1968. The infra-red determination of quartz in sediments and sedimentary rocks. *Chem. Geol.,* 3:199–212.

Deaton, B.C., 1987. Quantification of rock color from Munsell chips. *J. Sediment. Petrol.,* 57:774–776.

Deaton, B.C., and Balsam, W.L., 1991. Visible spectroscopy: a rapid method for determining hematite and goethite concentrations in geological materials. *J. Sediment. Petrol.,* 61:628–632.

Deaton, B.C., Nestell, M., and Balsam, W.L., 1996. Spectral reflectance of conodonts: a step toward quantitative color alteration and thermal maturity indexes. *AAPG Bull.,* 80:999–1007.

Giosan, L., Flood, R.D., Grützner, J., Franz, S.-O., Poli, M.-S., and Hagen, S., 2001. High-resolution carbonate content estimated from diffuse spectral reflectance for Leg 172 sites. *In* Keigwin, L.D., Rio, D., Acton, G.D., and Arnold, E. (Eds.), *Proc. ODP, Sci. Results,* 172, 1–12 [CD-ROM]. Available from: Ocean Drilling Program, Texas A&M University, College Station TX, 77854-9547, USA.

Goddard, E.N., Trask, P.D., De Ford, R.K., Rove, O.N., Singewald, J.T., and Overbeck, R.M., 1979. Rock color chart. *Geol. Soc. Am.*

Herbert, T.D., Tom, B.A., and Burnett, C., 1992. Precise major component determinations in deep-sea sediments using Fourier Transform Infrared Spectroscopy. *Geochim. Cosmochim. Acta,* 56:1759–1763.

Jones, G.A., and Kaiteris, P., 1983. A vacuum-gasometric technique for rapid and precise analysis of calcium carbonate in sediments and soils. *J. Sediment. Petrol.,* 53:655–660.

Mix, A.C., Harris, S.E., and Janecek, T.R., 1995. Estimating lithology from nonintrusive reflectance spectra: Leg 138. *In* Pisias, N.G., Mayer, L.A., Janecek, T.R., Palmer-

Julson, A., and van Andel, T.H. (Eds.), *Proc. ODP, Sci. Results,* 138: College Station, TX (Ocean Drilling Program), 413–427.

Mix, A.C., Rugh, W., Pisias, N.G., Veirs, S., Leg 138 Shipboard Sedimentologists (Hagelberg, T., Hovan, S., Kemp, A., Leinen, M., Levitan, M., Ravelo, C.), and Leg 138 Scientific Party, 1992. Color reflectance spectroscopy: a tool for rapid characterization of deep-sea sediments. *In* Mayer, L., Pisias, N., Janecek, T., et al., *Proc. ODP, Init. Repts.,* 138 (Pt. 1): College Station, TX (Ocean Drilling Program), 67–77.

O'Brien, P.E., Cooper, A.K., Richter, C., et al., 2001. *Proc. ODP, Init. Repts.,* 188 [CD-ROM]. Available from: Ocean Drilling Program, Texas A&M University, College Station TX 77845-9547, USA.

Schneider, R.R., Cramp, A., Damuth, J.E., Hiscott, R.N., Kowsmann, R.O., Lopez, M., Nanayama, F., Normark, W.R., and Shipboard Scientific Party, 1995. Color-reflectance measurements obtained from Leg 155 cores. *In* Flood, R.D., Piper, D.J.W., Klaus, A., et al., *Proc. ODP, Init. Repts.,* 155: College Station, TX (Ocean Drilling Program), 697–700.

Shipboard Scientific Party, 2001. Leg 188 summary: Prydz Bay–Cooperation Sea, Antarctica. *In* O'Brien, P.E., Cooper, A.K., Richter, C., et al., *Proc. ODP, Init. Repts.,* 188: College Station TX (Ocean Drilling Program), 1–65.

APPENDIX

Spectral values determined for each sample analyzed using the PerkinElmer Lambda 6 spectrophotometer at the University of Texas at Arlington are given in Table AT1. The table gives percent reflectance measured for each wavelength at 10-nm increments from 250 to 850 nm.

AT1. Spectral values, p. 49.

Figure F1. Calcium carbonate content (blue) and brightness (red) curves for the HiRISC section (0–54 mbsf) of Hole 1165B (sample measurements are listed in Table T1, p. 47).

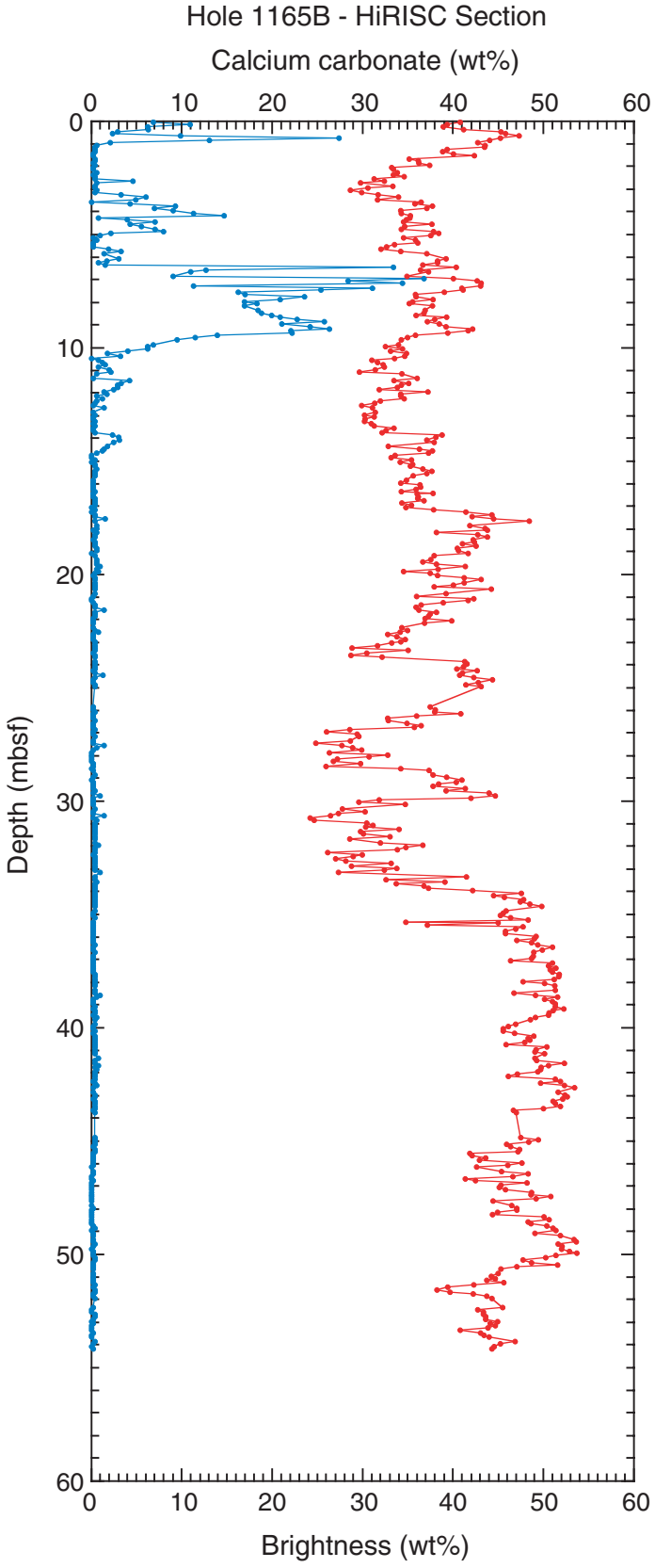

Figure F2. Curves showing changes in brightness down the HiRISC Section (0–54 mbsf) of Hole 1165B. The red curve was determined from dry, ground-up core samples using the PerkinElmer Lambda 6 Spectrophotometer, whereas the green curve was determined from shipboard measurements on wet cores using the Minolta CM-2002 Spectrophotometer. See "HiRISC Section," p. 5, in "Sediment Brightness Determined from Spectral Data" for details (sample measurements are listed in Table T2, p. 48).

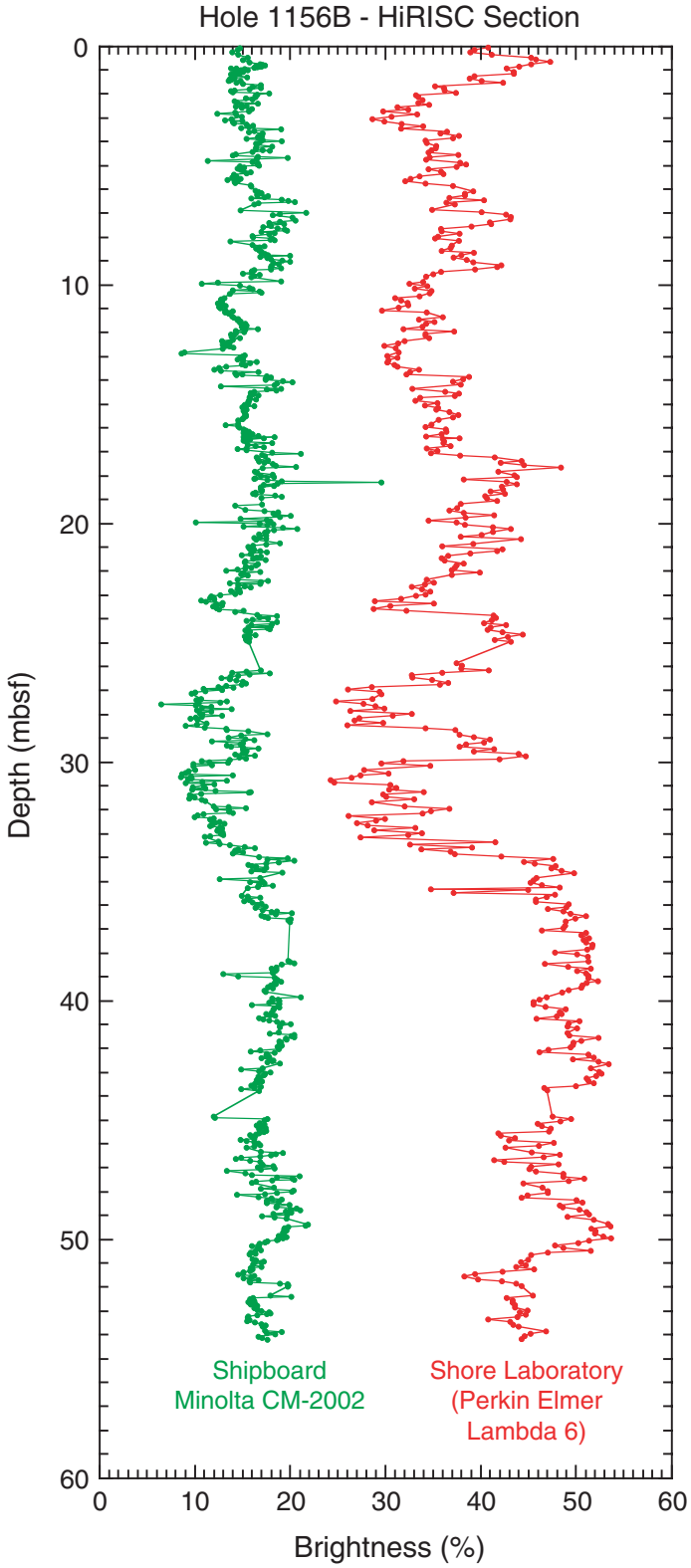

Figure F3. Percent reflectance for six color bands (violet, blue, green, yellow, orange, and red) down the HiRISC section (0–54 mbsf) of Hole 1165B (sample measurements are listed in Table T1, p. 47).

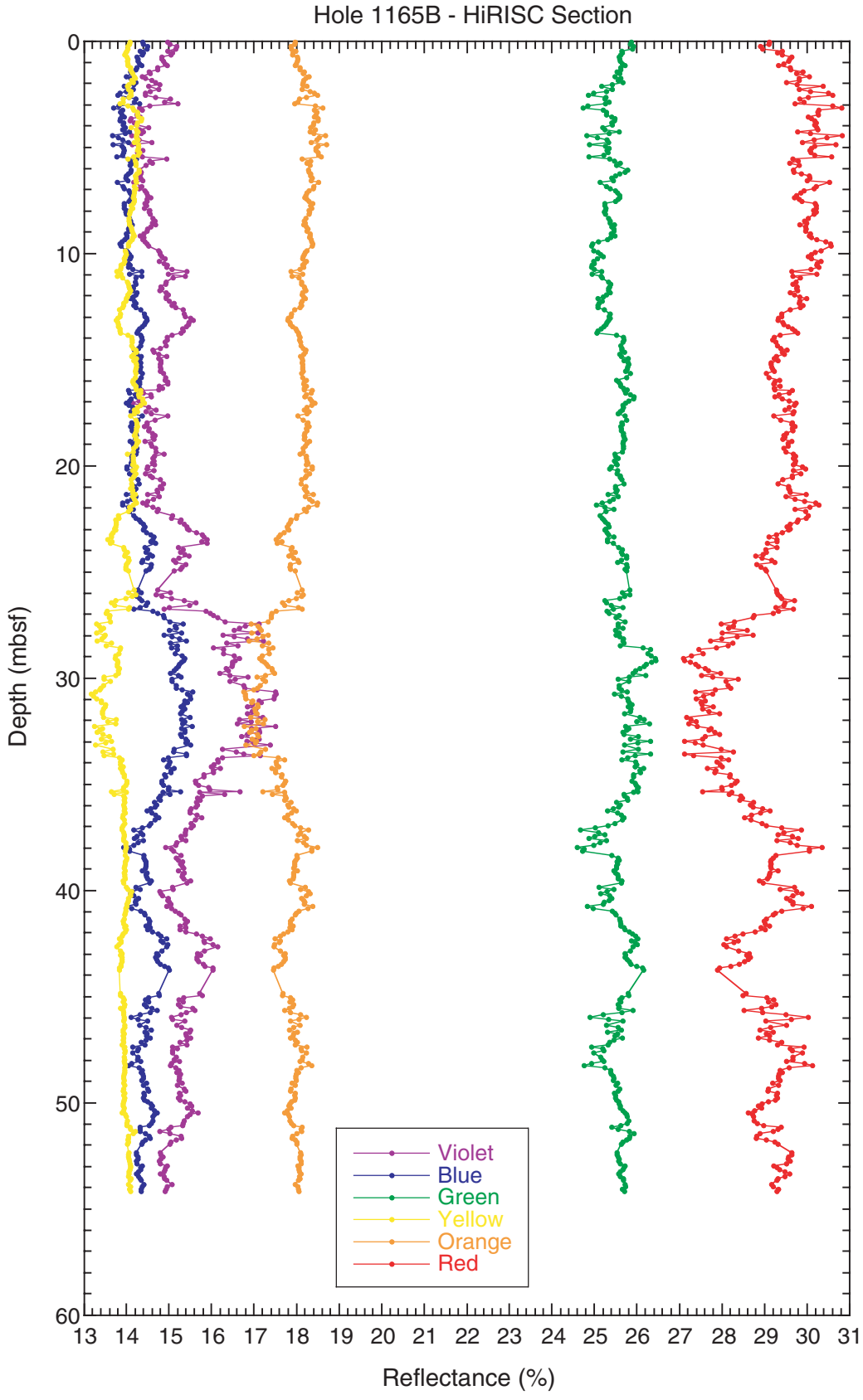

Figure F4. Brightness down Site 1165, Wild Drift (sample measurements are listed in Table T1, p. 47).

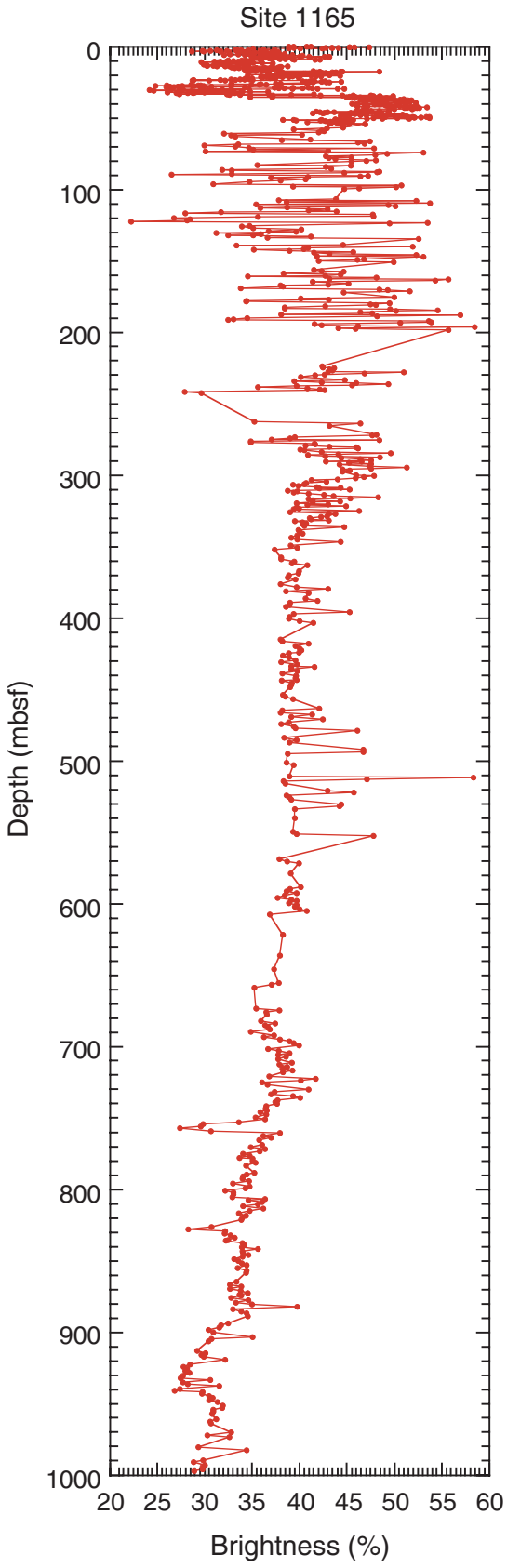

Figure F5. Percent reflectance for six color bands (violet, blue, green, yellow, orange, and red) down Site 1165 (sample measurements are listed in Table T1, p. 47).

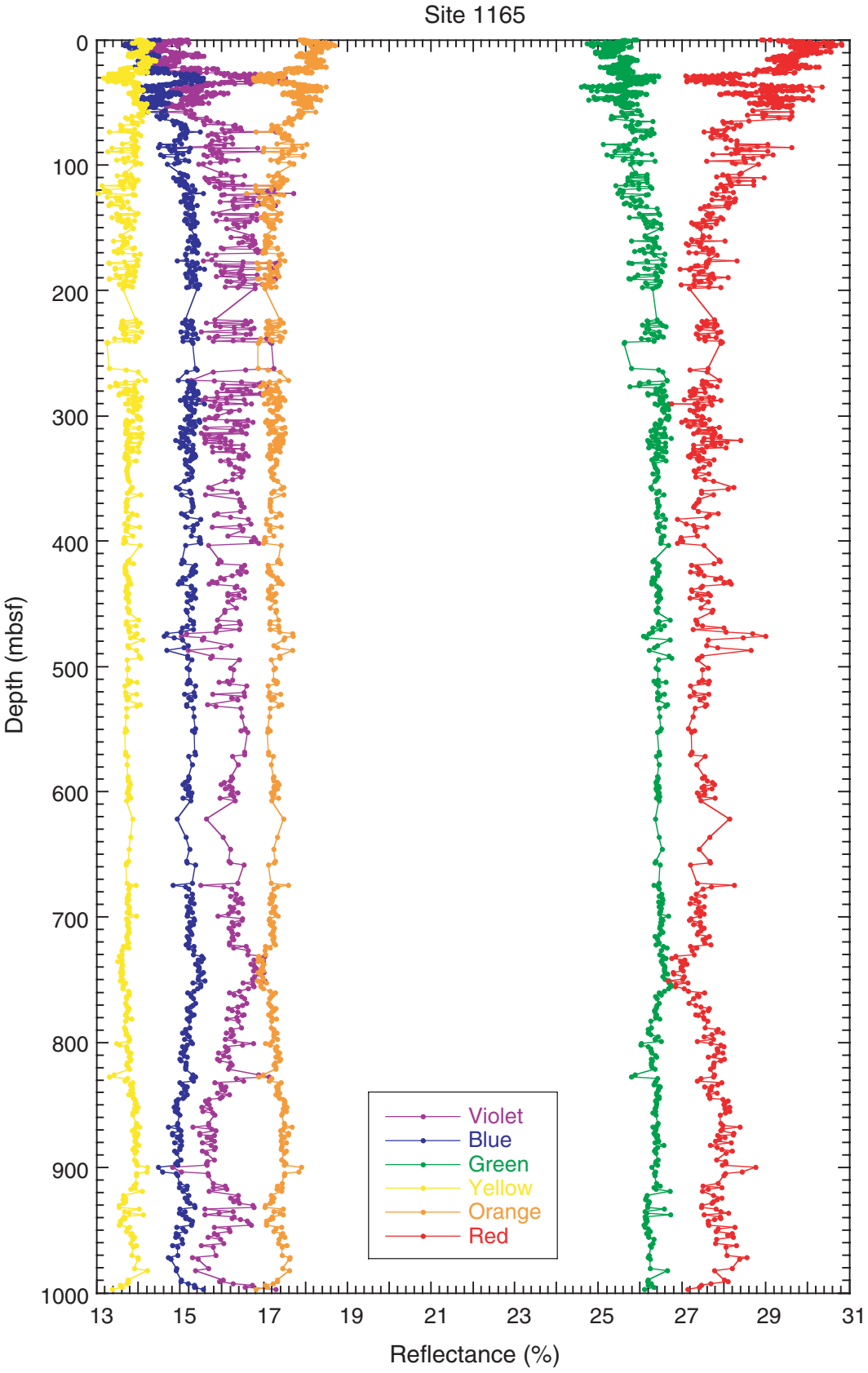

Figure F6. Brightness down Hole 1167A on Prydz Channel Trough-Mouth Fan (sample measurements are listed in Table T1, p. 47).

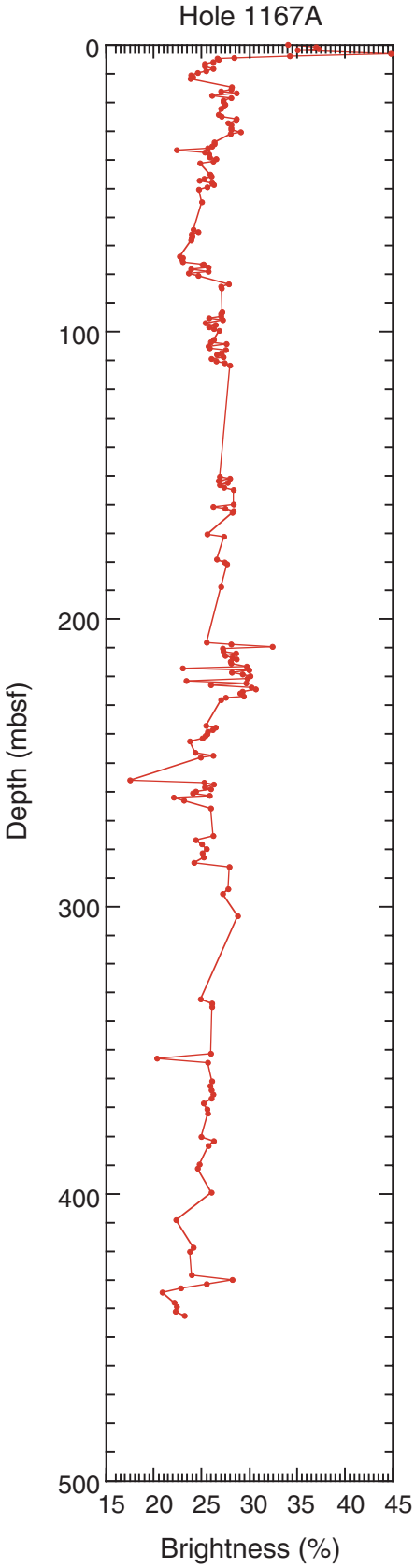

Figure F7. Percent reflectance for six color components (violet, blue, green, yellow, orange, and red) down Hole 1167A (sample measurements are listed in Table T1, p. 47).

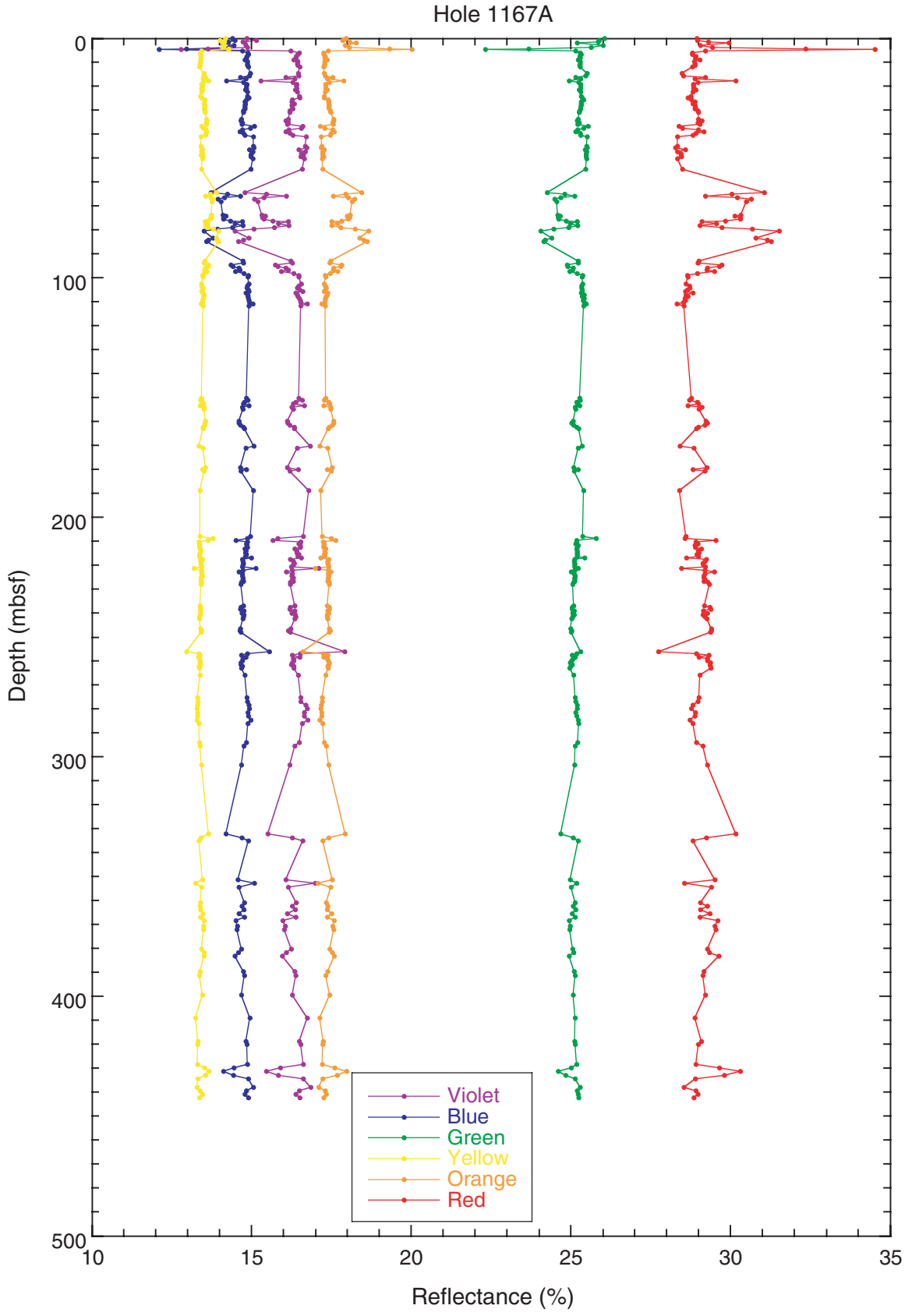

Figure F8. Example showing how a first-derivative curve (red triangles) derived from a percent reflectance curve (green circles) is used to more clearly identify peaks diagnostic of minerals, in this case hematite and goethite.

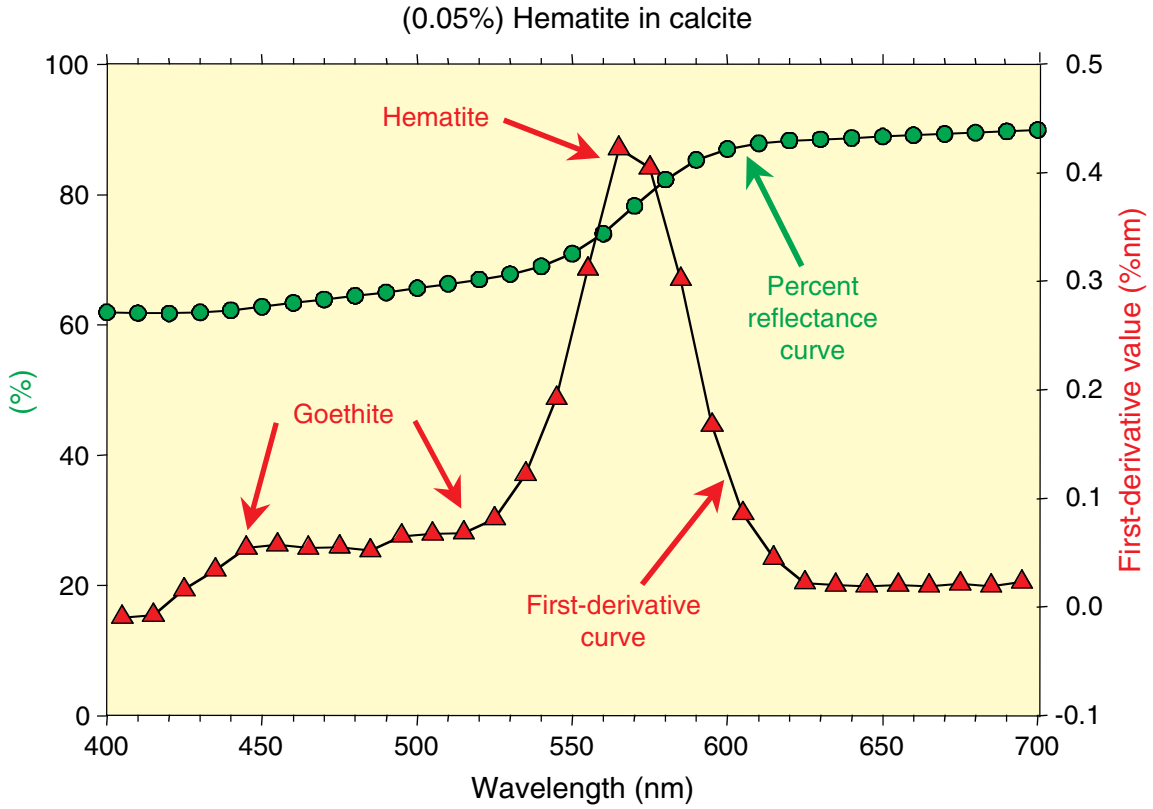

Figure F9. Example of interpretation of a factor description curve by comparison to the first-derivative curve (shown in Fig. F8, p. 24) from a known sample containing hematite and goethite (from Balsam et al., 1997). Squares = first-derivative values, circles = factor loading.

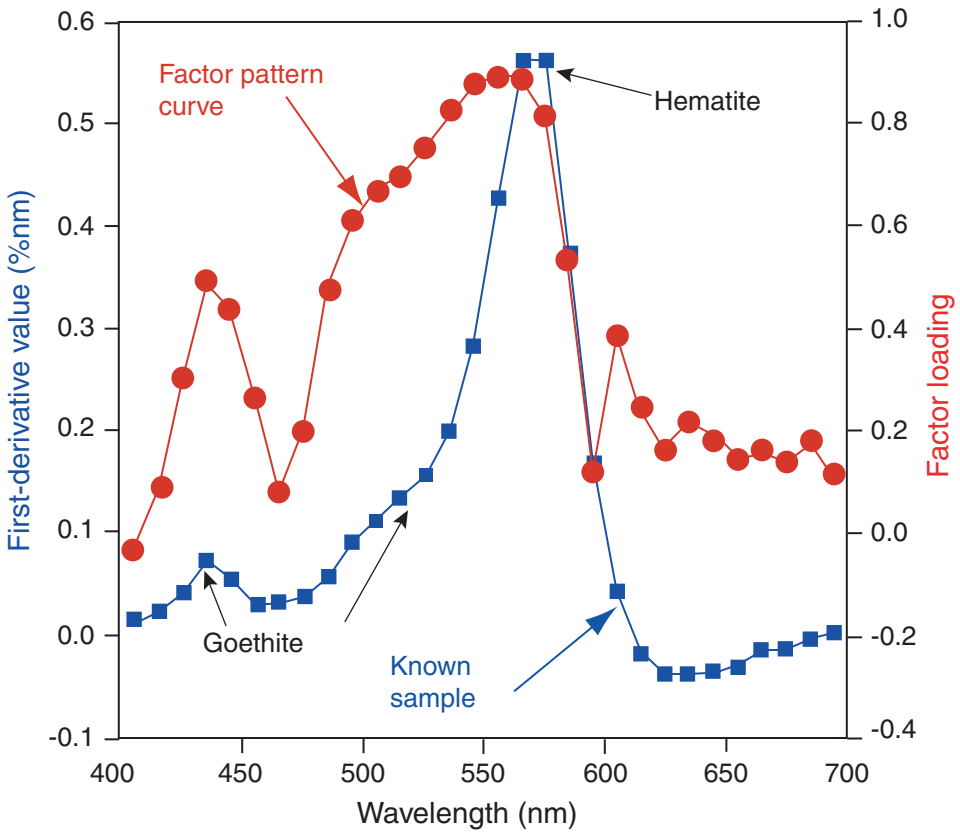

Figure F10. Factor 1 is interpreted as representing a combination of minerals including goethite and chlorite, most likely ripidolite. **A, B.** This interpretation is based on comparison of the first-derivative peaks derived from spectral analysis of standards to peaks in the factor loading curve. Our standard goethite is Hoover Color Corporation Synox HYG10, yellow, and is a manufactured sample. Ripidolite, one of our natural chlorite standards, is sample CGA-2 from the Clay Minerals Repository and is from Flagstaff Hill, California. (Continued on next page.)

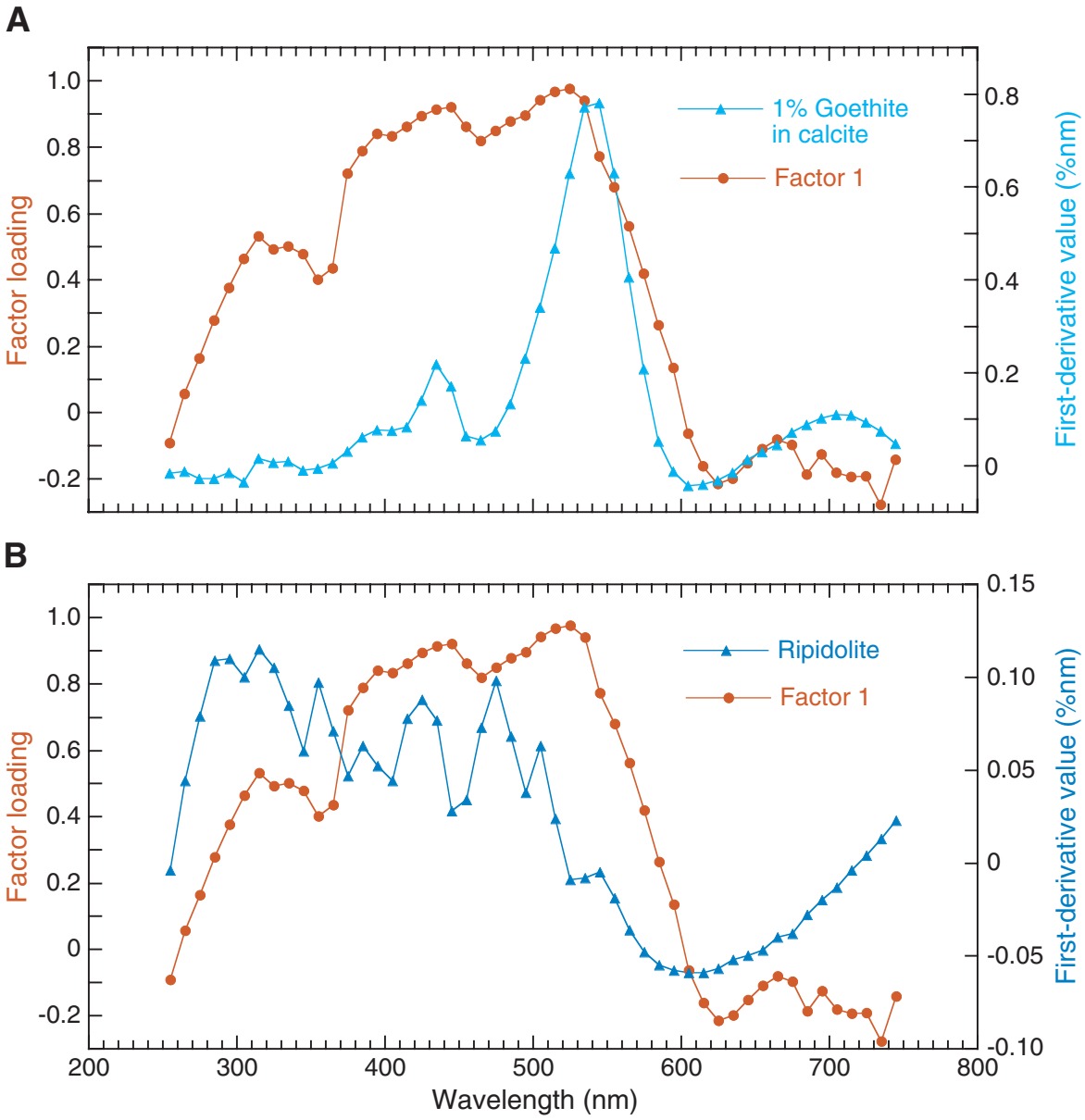

Figure F10 (continued). C. This curve clearly demonstrates the spectral dominance of goethite, even at low concentrations, and how the intermixing of two minerals may affect their combined spectrum. The silica and calcite in the known mineral mixture shown are white and do not influence the spectrum in the wavelength range we analyzed.

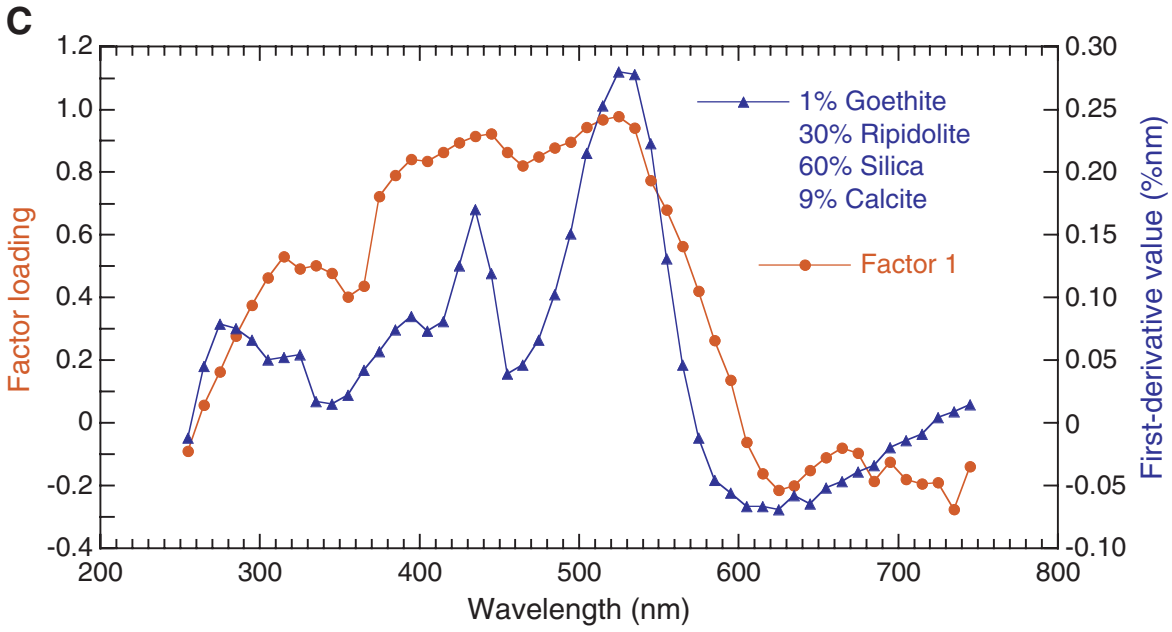

Figure F11. Factor 2 is interpreted as an organic matter factor. This interpretation is based on comparison of the factor loading curve for Factor 2 to the spectral curve of a small amount of lignite (0.1%) mixed with commercial topsoil. Note: We do not mean to imply that ocean-floor sediments contain material similar to topsoil, rather we use this mixture because we imply that this factor contains both mature, refractory organic matter and immature, young organic matter such as that found in topsoil.

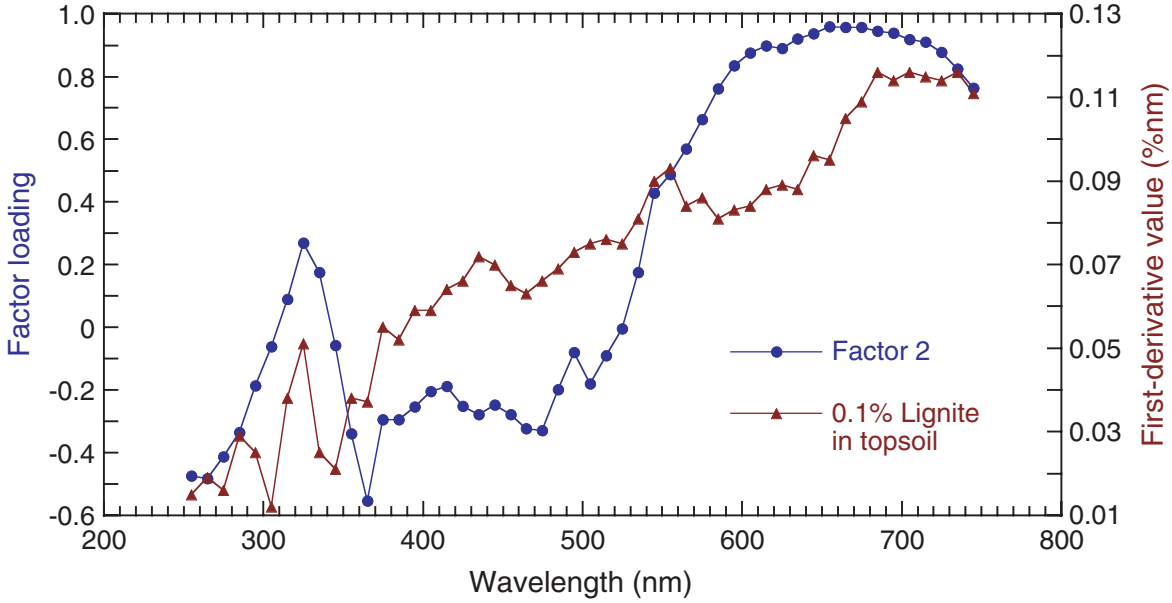

Figure F12. Factor 3 is interpreted as being influenced by both illite and montmorillonite. Comparison of the factor loading curve for Factor 3 to spectral patterns for (**A**) montmorillonite and (**B**) illite demonstrates that the factor loading curve shares first-derivative peaks with both of these clay minerals. Our montmorillonite sample is API 25 from Upton, Wyoming, and is described as 100% montmorillonite (bentonite). The illite sample is API 35 (Wards 46E-4100) from Fifthian, Illinois, and is described as 100% illite.

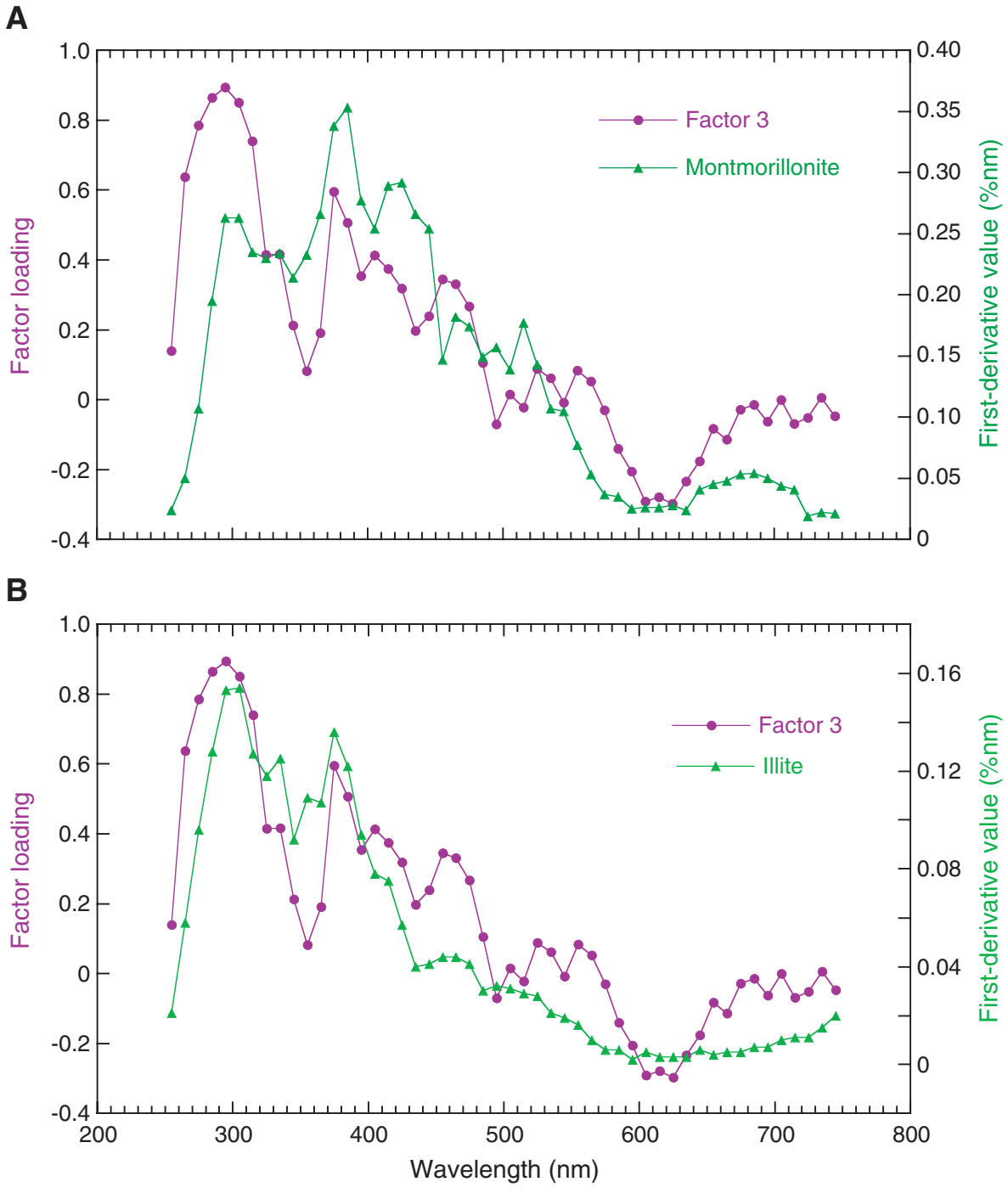

Figure F13. Factor 4 is interpreted as containing maghemite and some other undetermined mineral. The comparison of our factor loading curve to the first-derivative curve for a standard sample of maghemite displays several peaks in common. However, the 495-nm factor loading peak is not present in our standard and the maghemite first-derivative peak at 665 nm is not present on the factor loading curve; this suggests the presence of at least one additional mineral influencing the factor. Our maghemite standard is manufactured by Pfizer (their number 2230).

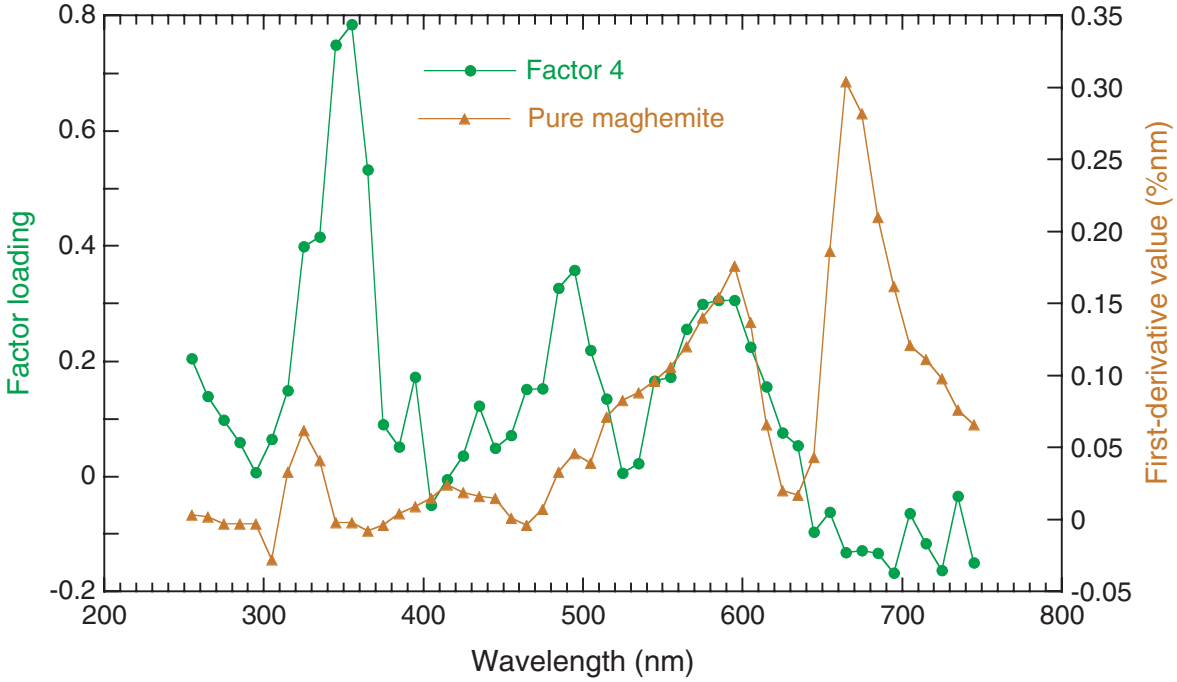

Figure F14. Factor 5 is interpreted as representing primarily hematite plus an unidentified mineral. The comparison of the factor loading curve to the first-derivative curve for 1% hematite in calcite clearly indicates the presence of hematite. However, the large factor loading peak at 335 nm and the smaller peaks centered around 400 nm indicate the presence of another mineral, probably a clay mineral, that has peaks in the NUV and shorter wavelengths of the VIS (for example see the curves for ripidolite, illite, and montmorillonite in previous figures).

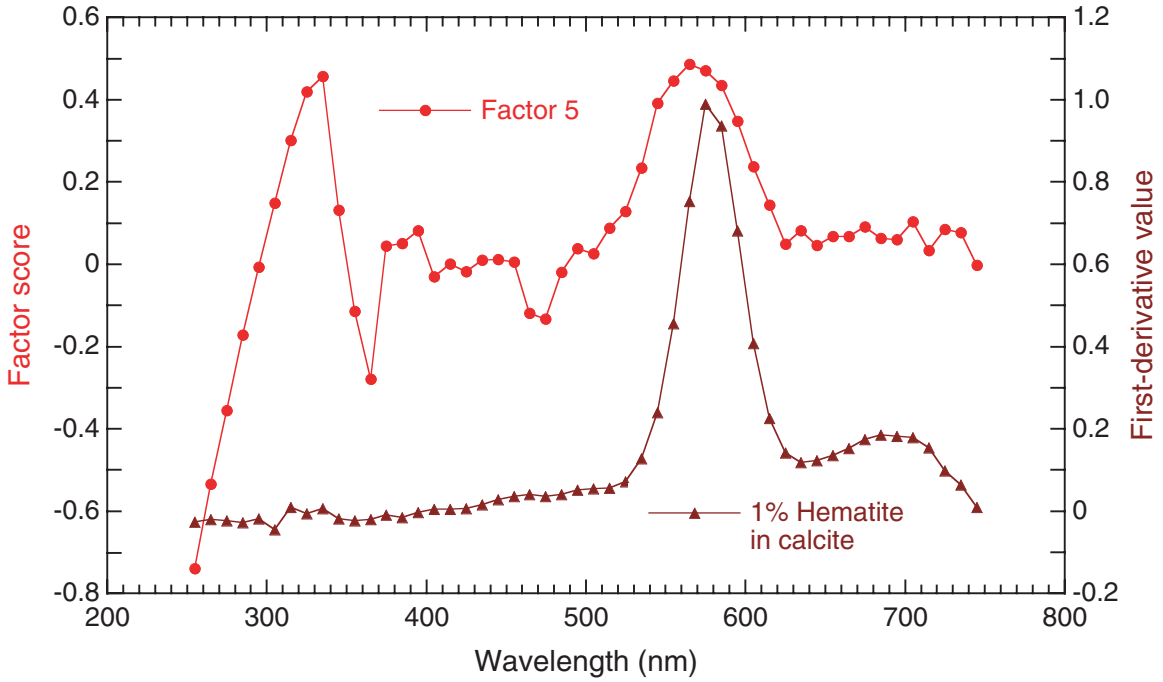

Figure F15. Factor scores for Factor 1 (goethite and ripidolite), Site 1165.

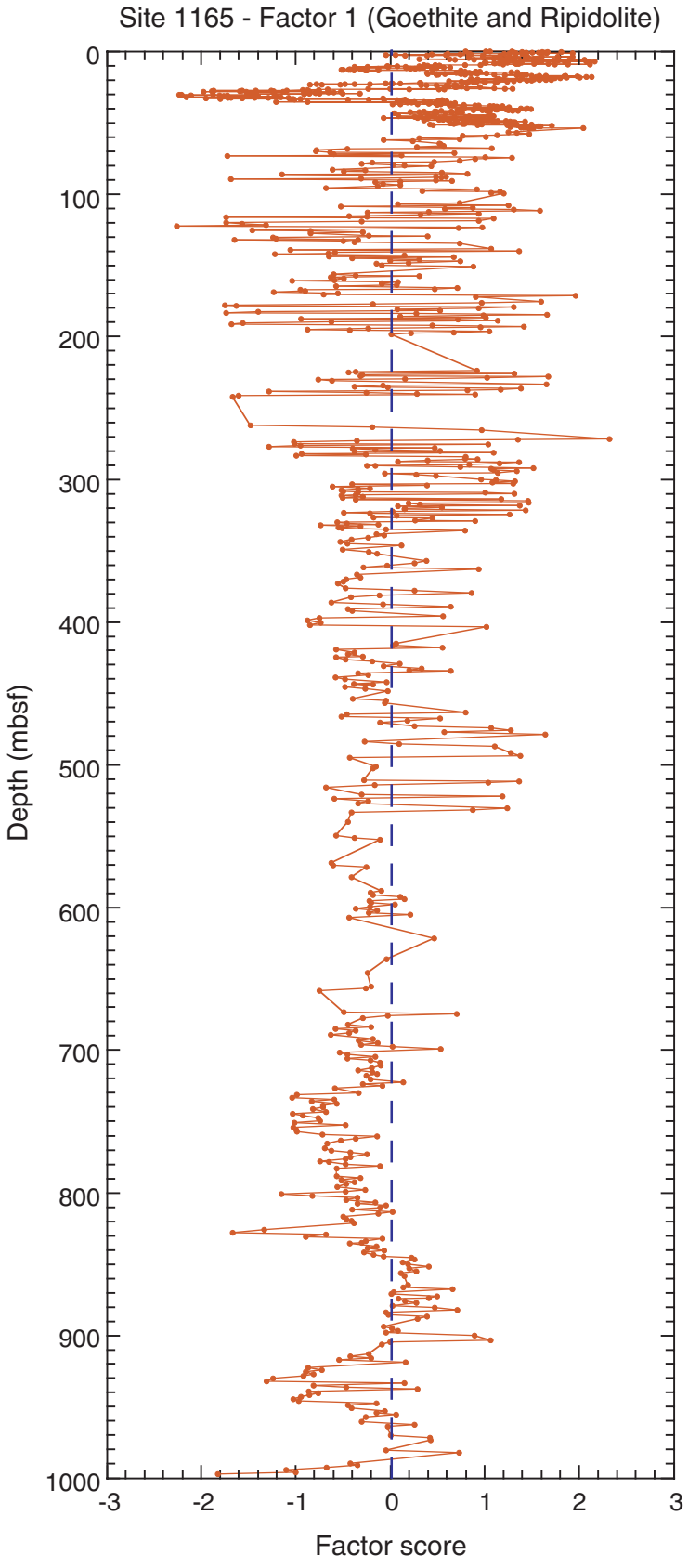

Figure F16. Factor scores for Factor 2 (organic matter), Site 1165.

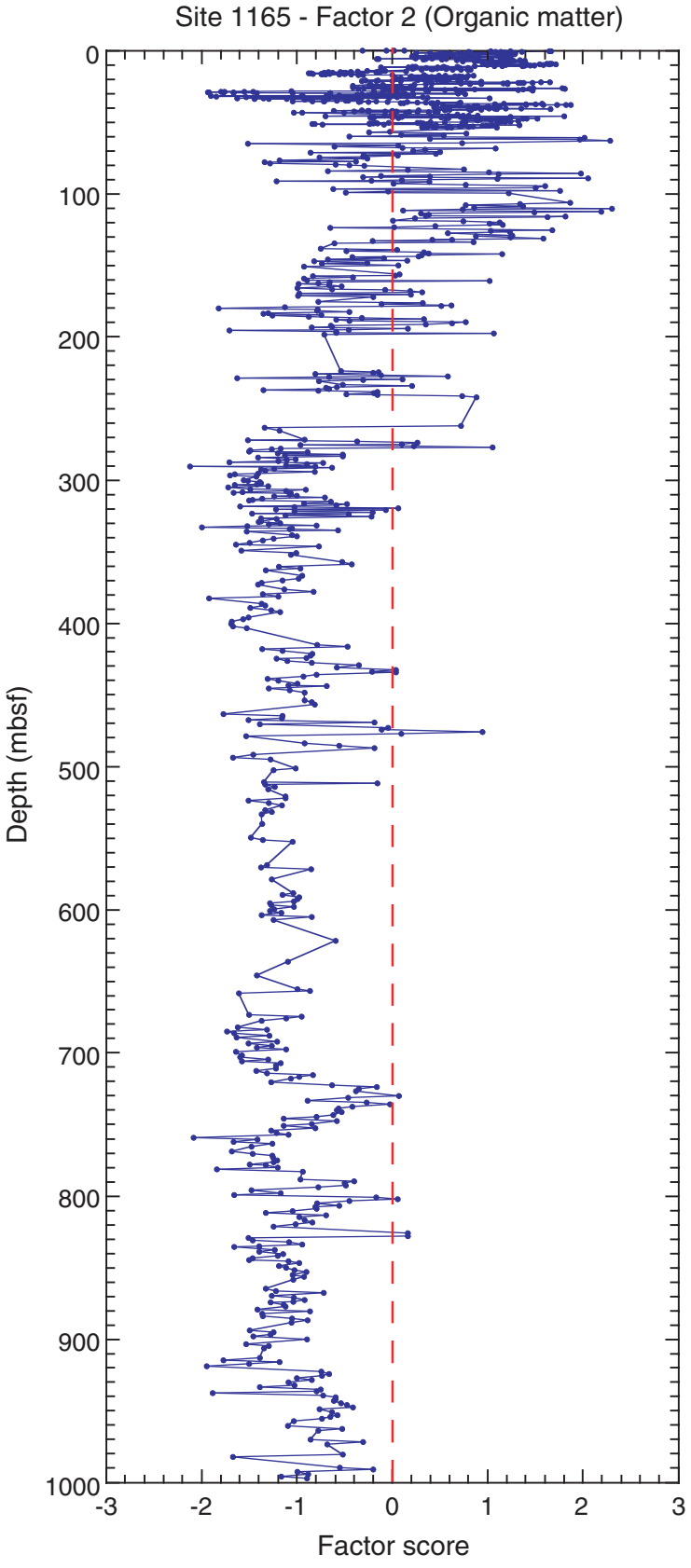

Figure F17. Factor scores for Factor 3 (montmorillonite and illite), Site 1165.

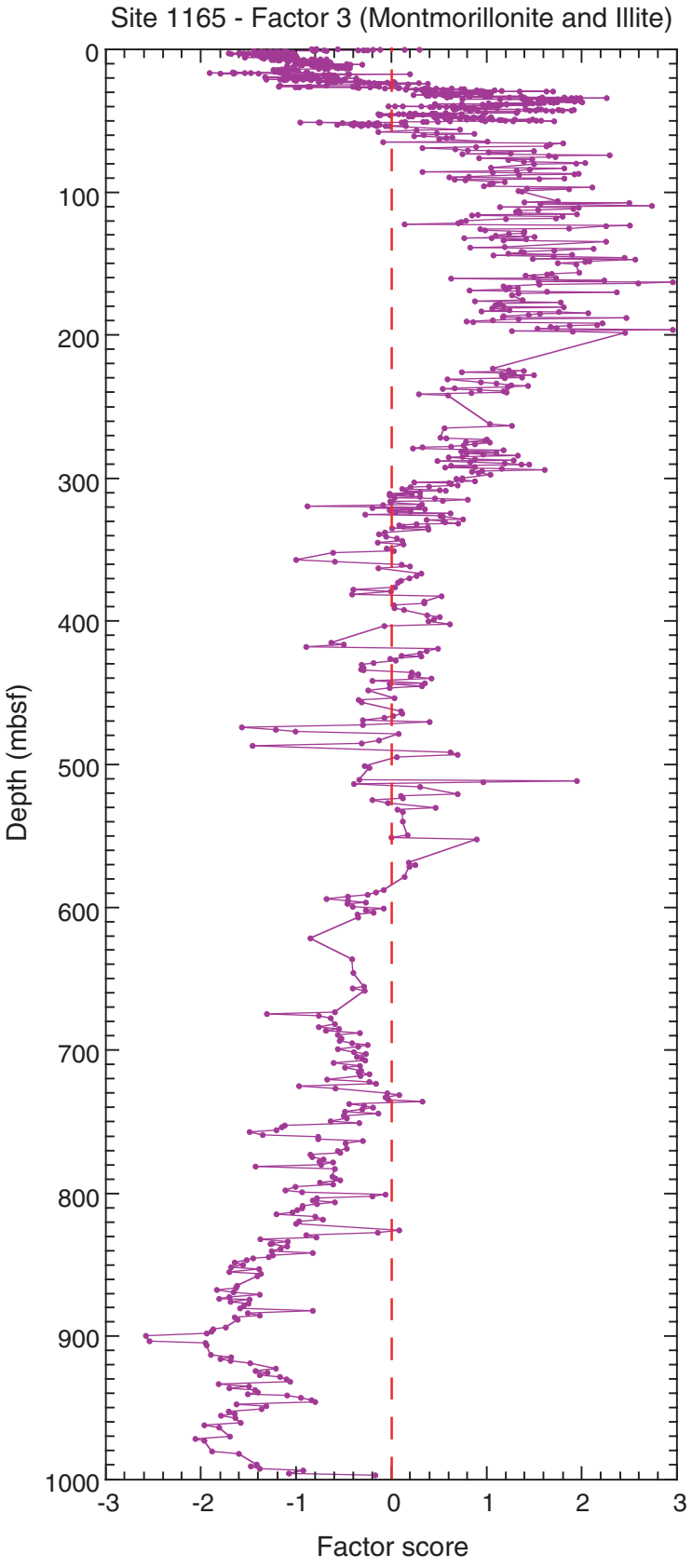

Figure F18. Factor scores for Factor 4 (maghemite), Site 1165.

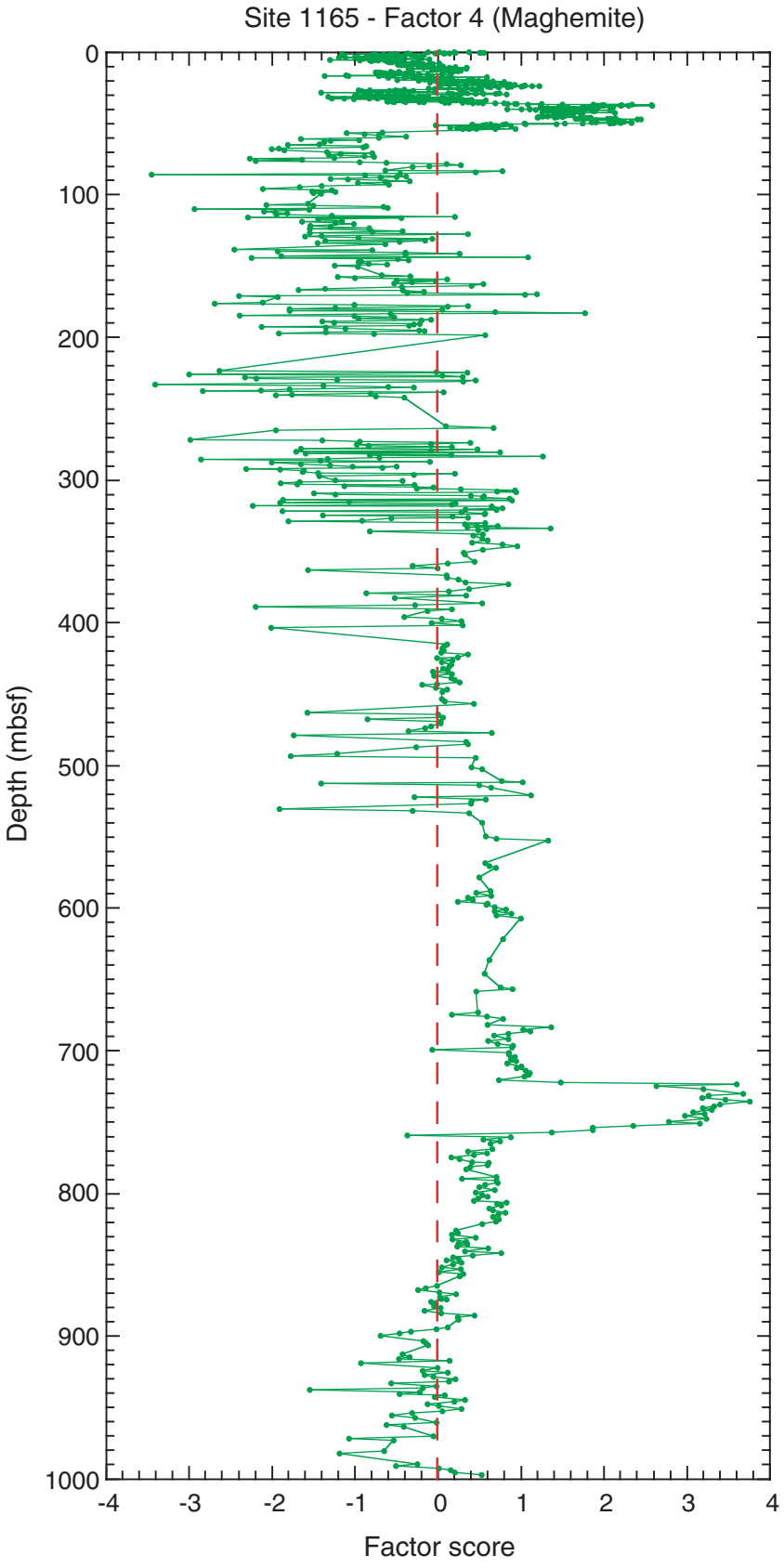

Figure F19. Factor scores for Factor 5 (hematite), Site 1165.

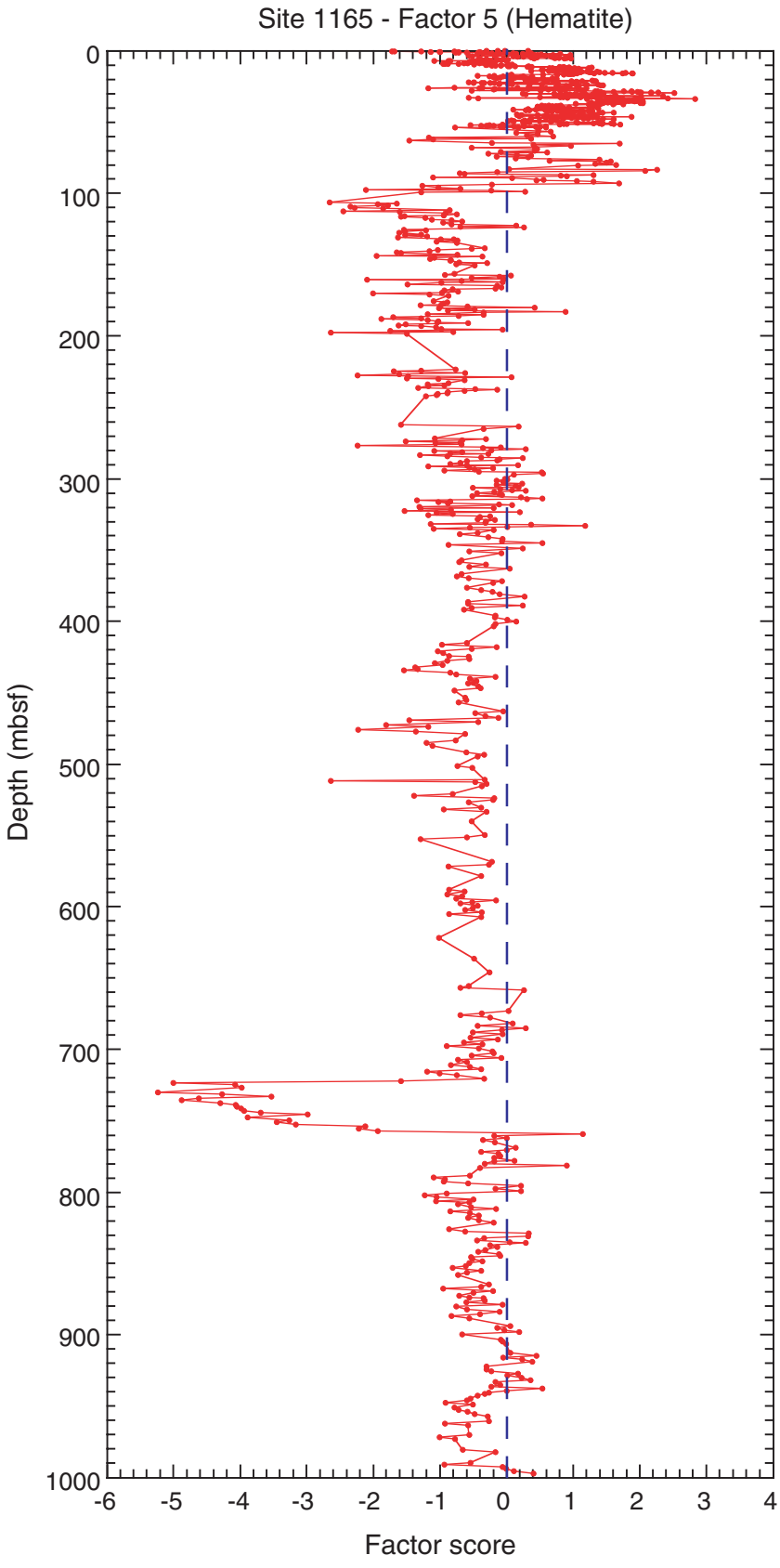

Figure F20. Factor scores for Factor 1 (goethite and ripidolite), HiRISC section of Hole 1165B.

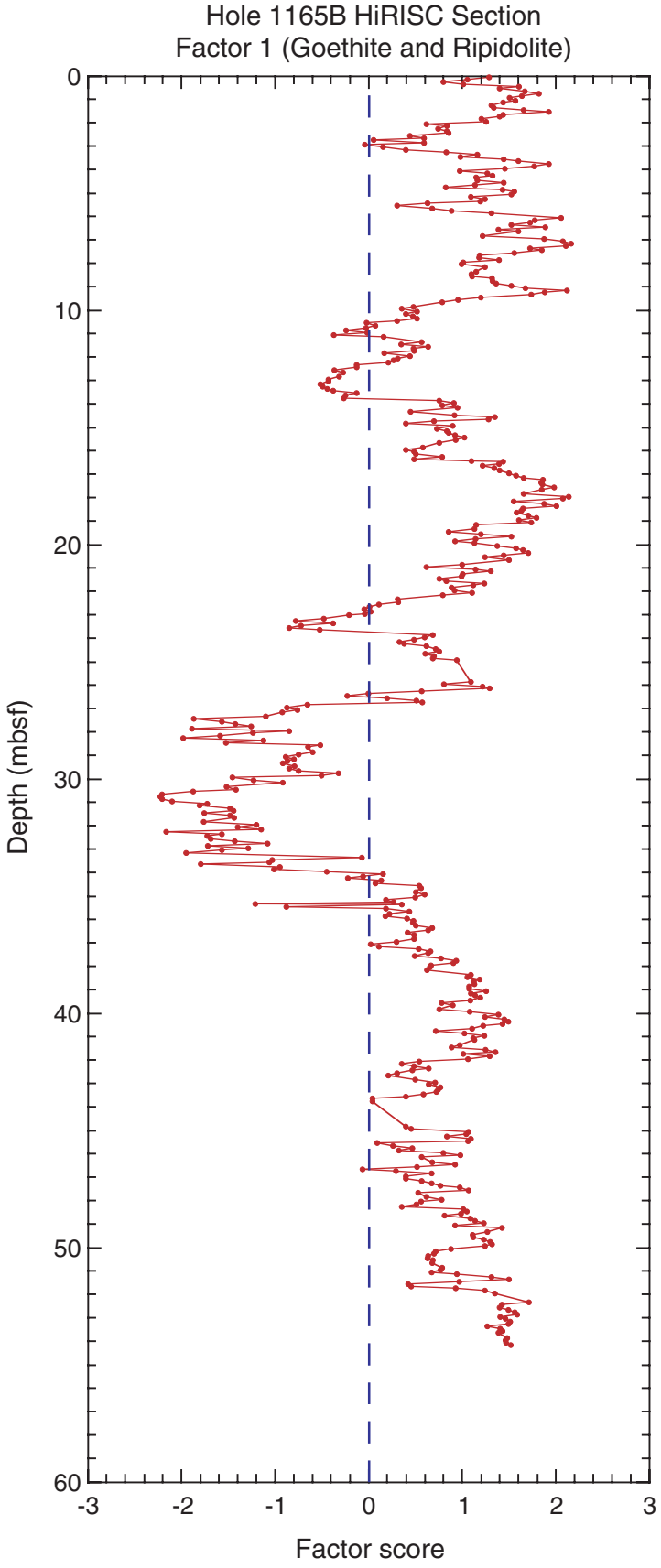

Figure F21. Factor scores for Factor 2 (organic matter), HiRISC section of Hole 1165B.

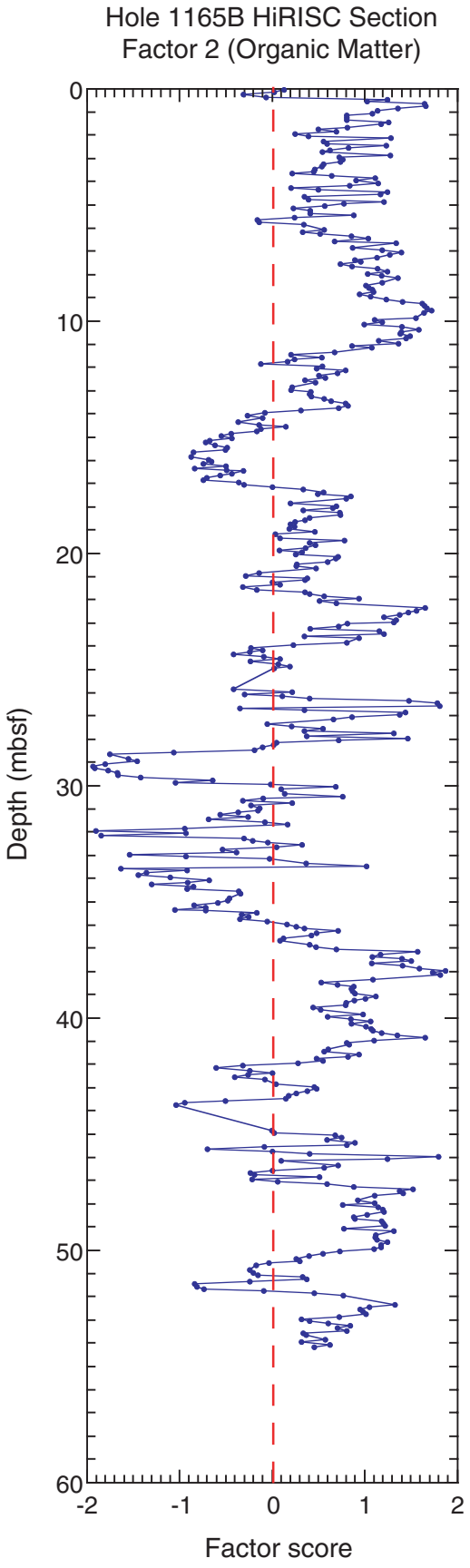

Figure F22. Factor scores for Factor 3 (montmorillonite and illite), HiRISC section of Hole 1165B.

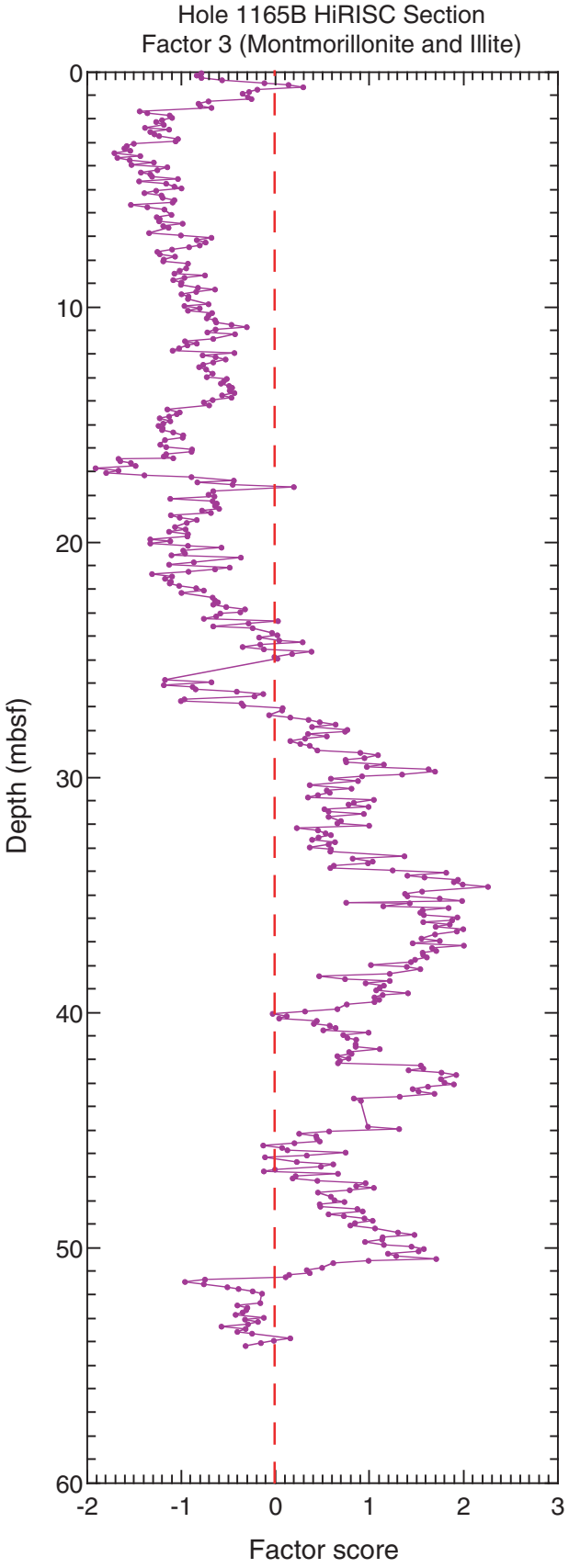

Figure F23. Factor scores for Factor 4 (maghemite), HiRISC section of Hole 1165B.

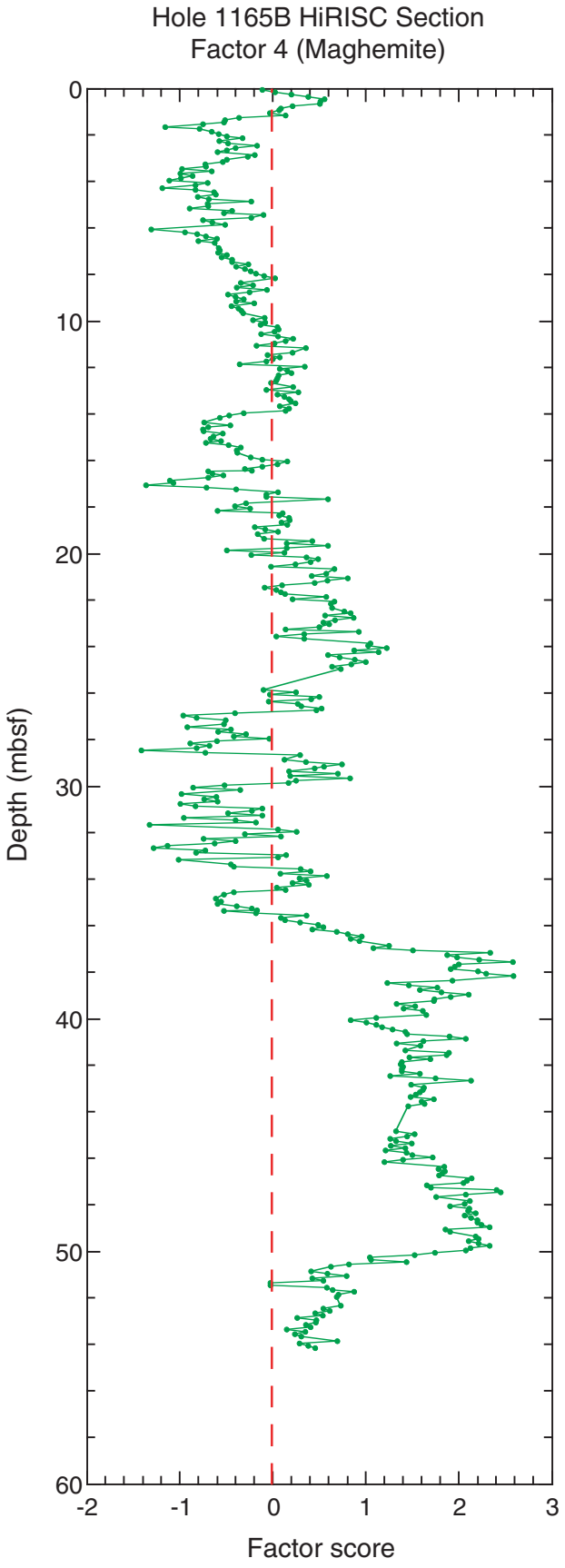

Figure F24. Factor scores for Factor 5 (hematite), HiRISC section of Hole 1165B.

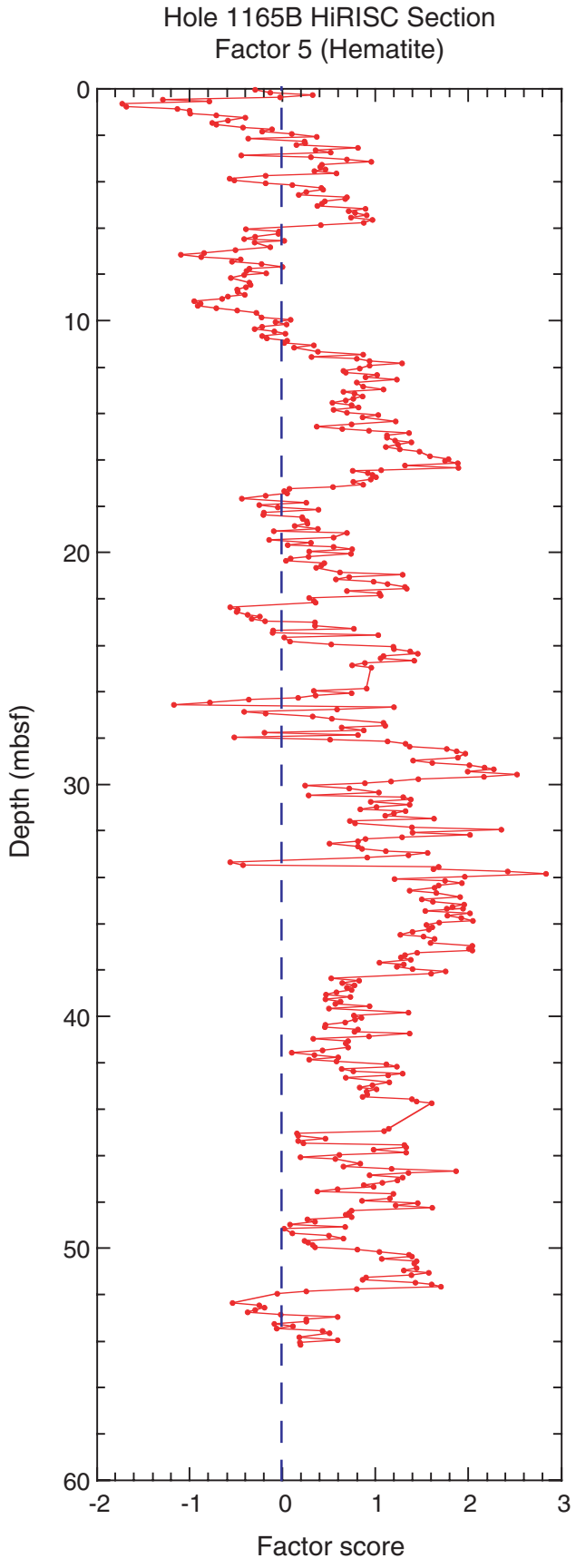

Figure F25. Factor scores for Factor 1 (goethite and ripidolite), Hole 1167A.

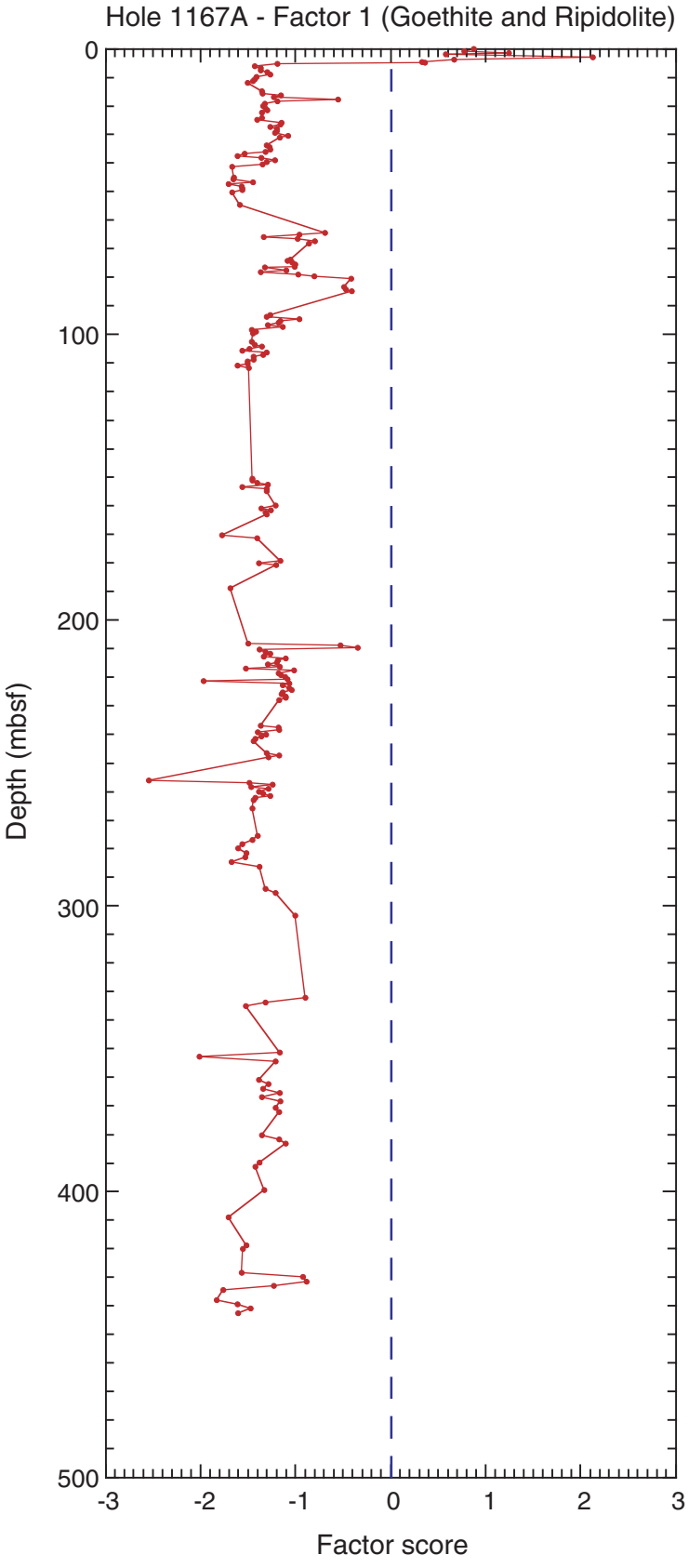

Figure F26. Factor scores for Factor 2 (organic matter), Hole 1167A.

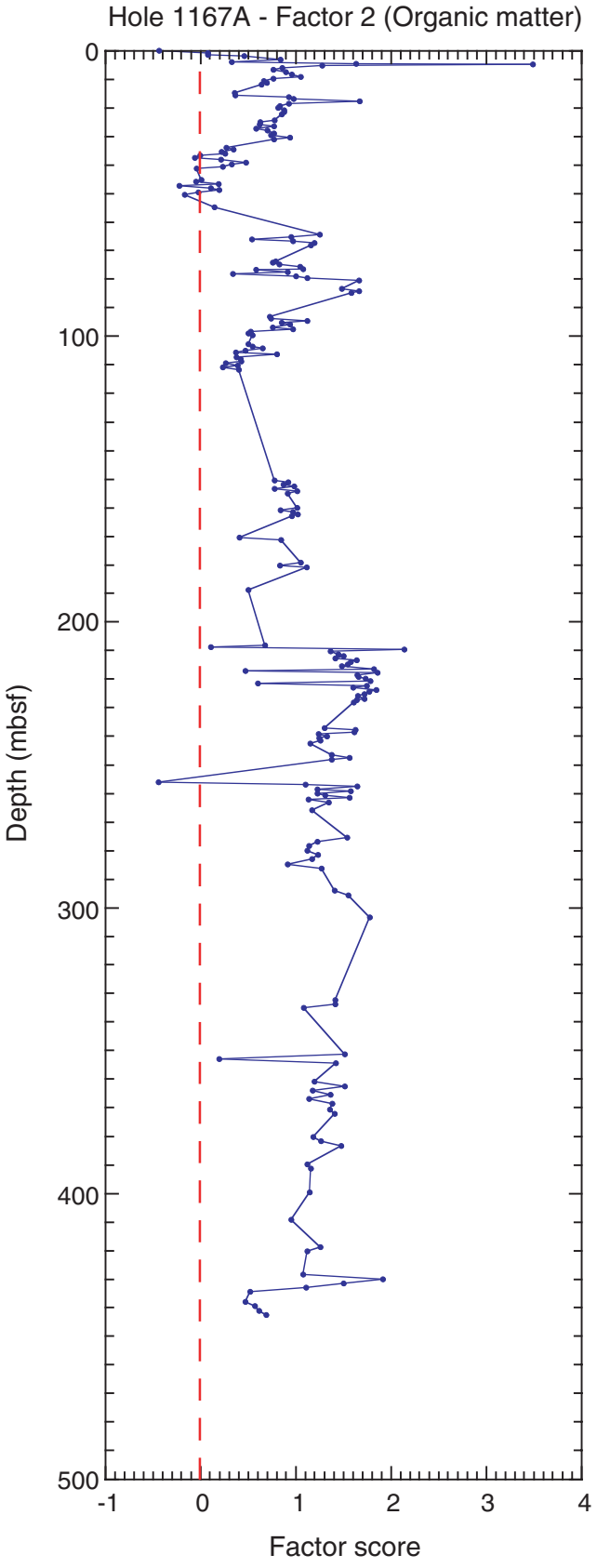

Figure F27. Factor scores for Factor 3 (montmorillonite and illite), Hole 1167A.

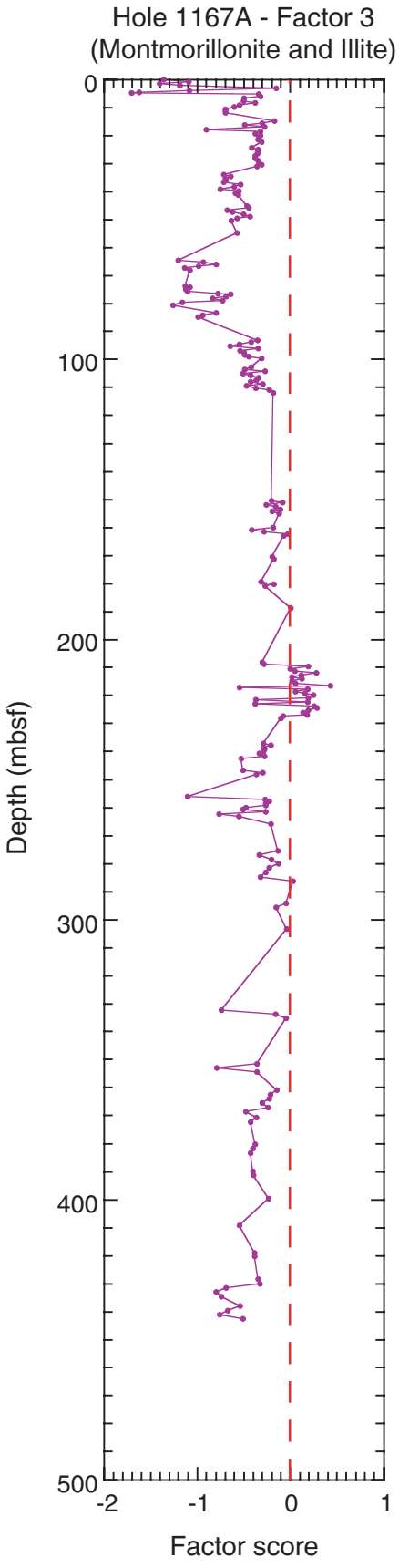

Figure F28. Factor scores for Factor 4 (maghemite), Hole 1167A.

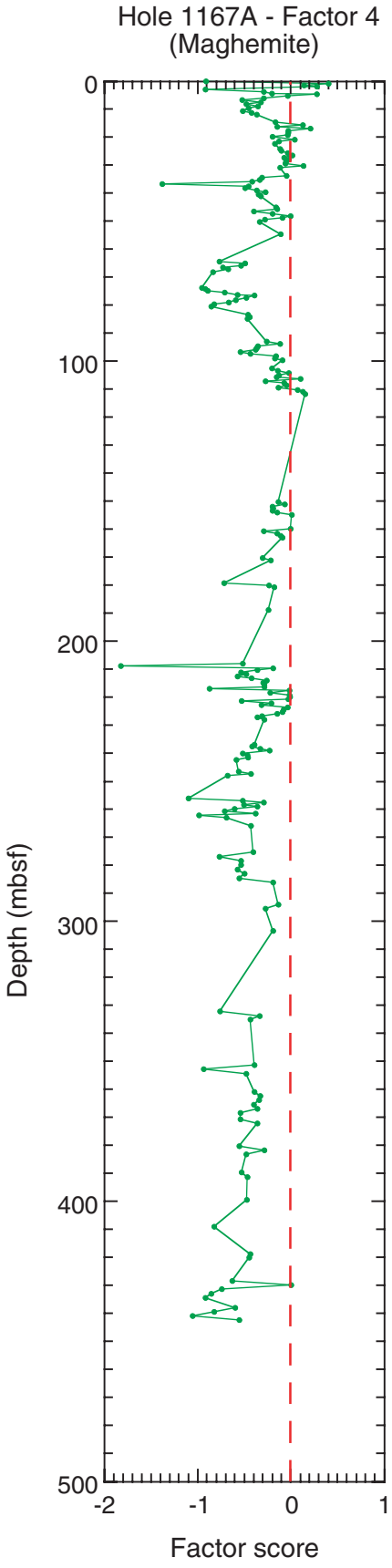

Figure F29. Factor scores for Factor 5 (hematite), Hole 1167A.

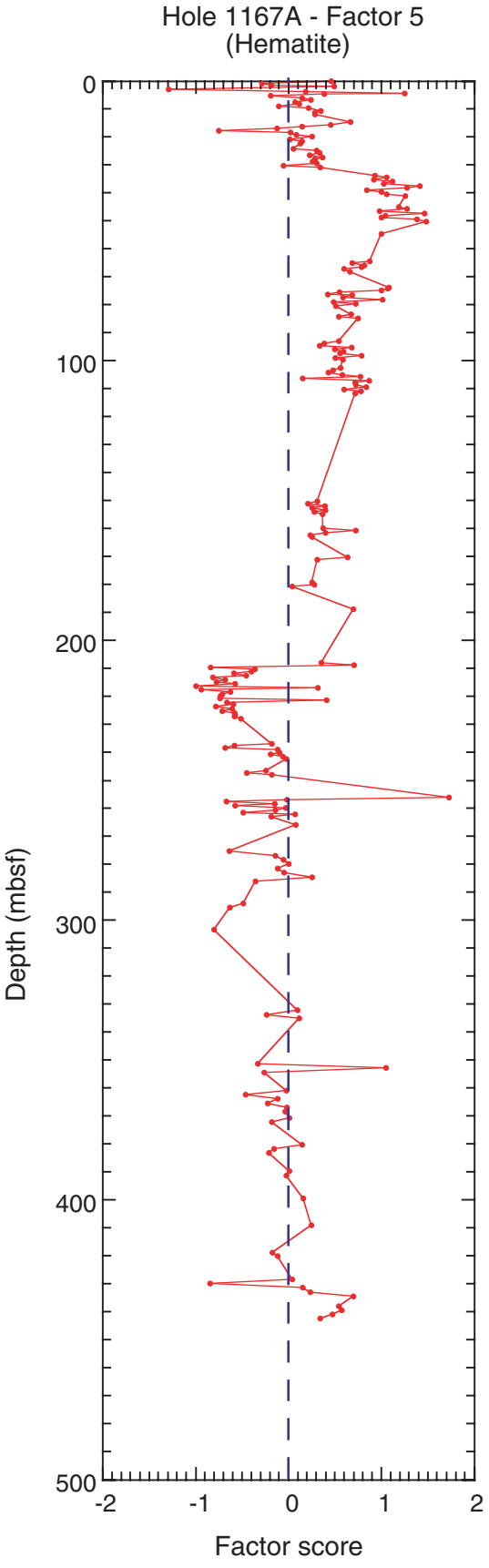

Table T1. Calcium carbonate content, brightness, percent brightness, percent reflectance for discrete color bands (violet, blue, green, yellow, orange, and red), and factor scores (Factors 1 through 5), Holes 1165B, 1165C, and 1167A.

Core, section, interval (cm)	Depth (mbsf)	$CaCO_3$ (wt%)	Brightness	Percent brightness	Color bands (%)						Factor scores					T^2	Probability
					Violet	Blue	Green	Yellow	Orange	Red	Factor 1	Factor 2	Factor 3	Factor 4	Factor 5		
188-1165B-																	
1H-1, 7–8	0.07	6.9	1263.91	40.77	14.97	14.39	25.87	14.09	17.96	29.12	1.2852	0.1295	–0.7826	0.1170	0.2948	2.3815	0.7952
1H-1, 17–18	0.17	10.9	1220.30	39.36	15.03	14.40	25.84	14.07	17.95	29.11	1.0565	0.0258	–0.8402	0.0215	0.1354	1.8415	0.8713
1H-1, 27–28	0.27	6.2	1205.18	38.88	15.17	14.50	25.92	14.04	17.87	28.90	0.7964	0.3128	0.7865	0.1985	0.3197	1.4922	0.9144
1H-1, 37–38	0.37	6.3	1277.31	41.20	15.15	14.49	25.90	14.03	17.88	28.95	1.0152	0.0620	0.5673	0.3799	0.0232	1.5012	0.9134
1H-1, 47–48	0.47	2.9	1403.73	45.28	14.97	14.32	25.65	14.01	17.98	29.42	1.6074	1.2421	0.1153	0.5577	1.2877	6.1091	0.2982
1H-1, 57–58	0.57	2.4	1420.32	45.82	15.09	14.40	25.66	13.98	17.92	29.30	1.3963	1.0316	0.1392	0.5114	0.7848	3.9107	0.5643
1H-1, 67–68	0.67	9.9	1467.15	47.33	15.05	14.37	25.62	13.96	17.91	29.42	1.6655	1.6488	0.2940	0.5007	1.7207	8.7905	0.1197
1H-1, 77–78	0.77	27.4	1403.10	45.26	14.83	14.25	25.58	14.01	18.02	29.64	1.8139	1.6666	0.1953	0.2101	1.6811	8.9760	0.1120
1H-1, 87–88	0.87	13.1	1365.74	44.06	14.83	14.27	25.60	14.04	18.03	29.59	1.6425	1.3596	0.2808	0.0871	1.1310	5.9118	0.3174
1H-1, 95–96	0.95	2.1	1325.85	42.77	14.87	14.27	25.60	14.03	18.02	29.56	1.5045	1.1385	0.3507	0.0680	1.0001	4.6877	0.4575
1H-1, 107–108	1.07	0.6	1348.39	43.50	14.90	14.31	25.66	14.03	17.99	29.46	1.5695	1.0832	0.2888	0.0330	0.9912	4.7034	0.4554
1H-1, 117–118	1.17	0.4	1346.79	43.44	14.96	14.36	25.72	14.04	17.96	29.33	1.4376	0.8069	0.2537	0.1369	0.7123	3.3084	0.6542
1H-1, 127–128	1.27	0.4	1220.18	39.36	14.73	14.24	25.62	14.10	18.08	29.61	1.3145	0.8052	0.7060	0.3621	0.3998	3.1656	0.6760
1H-1, 137–138	1.37	0.4	1204.28	38.85	14.74	14.21	25.62	14.09	18.08	29.61	1.3308	0.8070	0.8195	0.5127	0.5926	3.7077	0.5941
1H-1, 147–148	1.47	0.2	1242.52	40.08	14.53	14.10	25.53	14.13	18.18	29.90	1.6529	1.2575	0.8010	0.5265	0.7613	5.8118	0.3274
1H-2, 6–7	1.56	0.2	1313.51	42.37	14.55	14.16	25.59	14.16	18.16	29.76	1.9263	1.1801	0.6797	0.7550	0.7171	6.6495	0.2505
1H-2, 17–18	1.67	0.4	1089.82	35.16	14.37	13.99	25.48	14.18	18.29	30.06	1.4395	0.8105	1.4463	1.1588	0.4264	6.3454	0.2765
1H-2, 27–28	1.77	0.4	1121.73	36.18	14.44	14.10	25.62	14.20	18.23	29.80	1.4015	0.5004	1.3585	0.7843	0.1124	4.6879	0.4574
1H-2, 36–37	1.86	0.2	1122.89	36.22	14.59	14.13	25.55	14.13	18.17	29.80	1.2059	0.6966	1.1267	0.6527	0.2223	3.6844	0.5975
1H-2, 47–48	1.97	0.4	1158.87	37.38	14.69	14.21	25.68	14.16	18.15	29.51	1.2556	0.2502	1.0983	0.5858	0.1015	3.1987	0.6709
1H-2, 57–58	2.07	0.2	1030.39	33.24	14.78	14.17	25.42	14.06	18.14	29.77	0.6149	0.3934	1.2015	0.4898	0.3675	2.3514	0.7997
1H-2, 66–67	2.16	0.2	1035.83	33.41	14.52	13.94	25.17	14.03	18.25	30.39	0.8354	1.2875	–1.2700	–0.3220	0.3679	4.2072	0.5221
1H-2, 77–78	2.27	0.6	1050.68	33.89	14.77	14.17	25.42	14.05	18.13	29.81	0.7428	0.5567	–1.1806	–0.5787	0.2387	2.6472	0.7554
1H-2, 87–88	2.37	0.2	1036.84	33.45	14.56	14.00	25.28	14.11	18.31	30.09	0.8390	0.5905	–1.3854	–0.4814	0.2431	3.2628	0.6612
1H-2, 95–96	2.45	0.4	1072.33	34.59	14.45	13.85	24.99	14.10	18.42	30.50	0.8578	1.2315	–1.1302	–0.1691	0.1502	3.5809	0.6130
1H-2, 106.5–107.5	2.57	0.4	970.34	31.30	14.45	13.79	24.85	14.11	18.50	30.61	0.4421	0.8286	–1.3245	–0.4015	0.8079	3.4504	0.6326
1H-2, 116.5–117.5	2.66	4.6	1004.62	32.41	14.68	14.06	25.27	14.06	18.23	30.03	0.5919	0.6233	–1.2846	–0.4935	0.3558	2.7591	0.7383
1H-2, 126–127	2.76	0.6	923.70	29.80	15.03	14.22	25.24	13.92	18.06	29.83	0.0531	0.5460	–1.2327	–0.5955	0.5151	2.4403	0.7865
1H-2, 137–138	2.87	0.4	1034.26	33.36	14.89	14.19	25.34	13.91	18.03	29.93	0.5906	1.2795	–1.0334	–0.1902	–0.4466	3.2895	0.6571
1H-2, 145–146	2.95	0.4	950.18	30.65	15.21	14.30	25.26	13.85	17.95	29.72	–0.0423	0.7290	–1.0578	–0.2718	0.3064	1.8199	0.8741
1H-3, 6–7	3.06	0.6	888.98	28.68	14.54	13.83	24.84	14.04	18.44	30.60	0.1560	0.7584	–1.5016	–0.4943	0.6925	3.5783	0.6134
1H-3, 17–18	3.17	0.4	925.96	29.87	14.31	13.69	24.74	14.16	18.61	30.81	0.3915	0.7415	–1.5787	–0.5382	0.9536	4.3943	0.4963
1H-3, 27–28	3.27	3.3	983.13	31.71	14.38	13.90	25.21	14.18	18.42	30.28	0.8288	0.5592	–1.6033	–0.7281	0.4229	4.2792	0.5121
1H-3, 37–38	3.37	6.0	1052.11	33.94	14.25	13.86	25.29	14.25	18.48	30.25	1.1629	0.5368	–1.5395	–0.7219	0.4044	4.6954	0.4565
1H-3, 47–48	3.47	4.9	981.60	31.66	14.25	13.88	25.29	14.25	18.46	30.27	0.9796	0.4576	–1.7076	–0.9726	0.4662	5.2484	0.3887
1H-3, 57–58	3.57	0.0	1131.28	36.49	14.32	13.95	25.42	14.28	18.41	30.04	1.4427	0.4482	–1.4342	–0.6574	0.3425	4.8890	0.4319
1H-3, 67–68	3.67	4.3	1108.55	35.76	14.11	13.87	25.48	14.36	18.51	30.11	1.5985	0.2163	–1.6799	–0.9968	0.5804	6.7546	0.2420
1H-3, 77–78	3.77	9.3	1169.48	37.73	14.08	13.86	25.46	14.34	18.50	30.17	1.9298	0.6424	–1.5465	–0.8634	–0.1801	7.3065	0.2012
1H-3, 87–88	3.87	7.0	1149.13	37.07	14.18	13.93	25.42	14.25	18.40	30.21	1.7688	1.1113	–1.2945	–0.9850	–0.5700	7.3346	0.1993
1H-3, 96–97	3.96	9.0	1059.57	34.18	14.24	13.92	25.42	14.24	18.39	30.17	1.4552	0.9083	–1.5249	–1.1128	–0.5164	6.7732	0.2405
1H-3, 106.5–107.5	4.07	11.3	1063.45	34.30	14.52	13.97	25.19	14.11	18.32	30.22	0.9767	1.1492	–1.1492	–0.7002	–0.1775	4.1171	0.5347
1H-3, 117–118	4.17	14.7	1094.75	35.31	14.31	13.90	25.25	14.23	18.44	30.25	1.2691	0.8426	–1.2564	–0.8313	0.1041	4.6010	0.4687
1H-3, 127.5–128.5	4.28	0.8	1091.84	35.22	14.40	14.08	25.59	14.27	18.31	29.78	1.3285	0.2082	–1.4329	–1.1872	0.4162	5.4443	0.3665

Notes: Percent brightness is brightness rescaled to 100%. Note that carbonate content was determined only for samples from the HiRISC Section (0–54 mbsf) of Hole 1165B (see text for details). Only a portion of this table appears here. The complete table is available in **ASCII.**

Table T2. Percent brightness down the HiRISC section, Hole 1165B (0–54 mbsf).

Depth (mbsf)	Minolta (edited) percent brightness	PerkinElmer percent brightness
0.07		40.77
0.08	14.70	
0.17		39.36
0.18	14.48	
0.27		38.88
0.28	13.94	
0.37		41.20
0.38	14.59	
0.47		45.28
0.48	15.54	
0.57		45.82
0.58	15.05	
0.67		47.33
0.68	15.75	
0.77		45.26
0.78	16.86	
0.80	17.13	
0.82	17.37	
0.84	16.39	
0.86	16.71	
0.87		44.06
0.88	16.96	
0.90	16.52	
0.92	16.18	
0.94	14.40	
0.95		42.77
0.96	13.80	
0.98	15.24	
1.00	14.30	
1.02	14.86	
1.04	15.55	
1.06	15.03	
1.07		43.50
1.08	15.03	
1.10	14.15	
1.12	14.38	
1.14	14.73	
1.16	14.51	
1.17		43.44
1.18	13.77	
1.20		
1.22		
1.24		
1.26		
1.27		39.36
1.28		
1.30		
1.32	15.50	
1.34	14.21	
1.36	13.98	
1.37		38.85
1.38	13.85	
1.40	13.69	
1.42	13.76	
1.44	13.67	
1.46	13.51	
1.47		40.08
1.48	14.77	
1.55	14.35	
1.56		42.37
1.60	15.05	
1.65	16.93	
1.67		35.16
1.70	16.10	
1.75	16.94	
1.77		36.18
1.80	15.74	
1.85	14.19	
1.86		36.22
1.90	13.78	
1.95	14.02	
1.97		37.38
2.00	17.75	
2.05	16.50	
2.07		33.24
2.10	16.35	
2.15	16.37	
2.16		33.41
2.20	15.36	
2.25	16.09	
2.27		33.89
2.30	14.19	
2.35	14.44	
2.37		33.45
2.40	16.61	
2.45	14.86	
2.45		34.59
2.50	15.41	
2.55	14.30	
2.57		31.30
2.60	14.88	
2.65	16.04	
2.66		32.41
2.70	15.76	
2.75	15.67	
2.76		29.80
2.80	14.25	
2.85	12.34	
2.87		33.36
2.90	14.38	
2.95	14.92	
2.95		30.65
3.05	13.83	
3.06		28.68
3.10	13.11	
3.15	14.97	
3.17		29.87
3.20	13.98	
3.25	14.12	
3.27		31.71
3.30	15.41	
3.35	16.17	
3.37		33.94
3.40	15.68	
3.45	14.82	
3.47		31.66
3.50	19.06	
3.55	16.21	
3.57		36.49
3.60	15.66	
3.65	17.09	
3.67		35.76
3.70	17.06	
3.75	17.03	
3.77		37.73
3.80	16.65	
3.85	16.61	
3.87		37.07
3.90	15.45	
3.95	17.11	
3.96		34.18
4.00	19.12	
4.05	16.77	
4.07		34.30
4.10	16.41	
4.15	16.48	
4.17		35.31
4.20	18.13	
4.25	16.42	
4.28		35.22
4.30	16.37	
4.35	17.13	
4.37		34.88
4.40	17.82	
4.45	16.09	
4.47		34.56
4.55	14.29	
4.57		37.64
4.60	14.00	
4.65	16.62	
4.67		34.65
4.70	19.72	
4.75	16.48	
4.77		34.27
4.80	11.36	
4.85	16.10	
4.87		37.86
4.90	16.61	
4.95	16.54	
4.97		38.46
5.00	16.71	
5.05	14.71	
5.07		37.50
5.10	15.15	
5.15	14.54	
5.17		34.56
5.20	14.80	
5.25	15.09	
5.27		35.82
5.30	15.91	
5.35	15.42	
5.37		36.08
5.40	14.10	
5.45	14.38	
5.46		33.56
5.50	13.91	
5.55	14.77	
5.57		32.63
5.60	13.39	
5.65	14.55	
5.67		32.07
5.70	14.18	
5.75	14.26	
5.77		34.22
5.80		
5.85	15.91	
5.88		37.10
5.90	15.96	
6.05	16.37	
6.07		39.22

Notes: Brightness was determined from both wet cores aboard the *JOIDES Resolution* with the Minolta CM-2002 spectrophotometer and from dry sediments in the UTA shore-based laboratory using the PerkinElmer Lambda 6 spectrophotometer. The Minolta values have been edited to exclude measurements made at core voids, gaps, etc. (see text for details). Only a portion of this table appears here. The complete table is available in **ASCII.**

Table AT1. Spectral values (percent reflectance).

Core, section, interval (cm)	Depth (mbsf)	Wavelength (nm)																					
		250	260	270	280	290	300	310	320	330	340	350	360	370	380	390	400	410	420	430	440	450	460
188-1165B-																							
1H-1, 7–8	0.07	8.10	8.26	8.90	9.94	11.36	13.03	14.73	16.69	19.04	20.33	20.78	21.64	22.67	24.54	26.16	27.63	29.17	30.99	32.53	33.79	35.09	35.83
1H-1, 17–18	0.17	7.70	7.86	8.51	9.53	10.92	12.55	14.15	16.00	18.53	19.70	20.17	21.02	22.06	23.79	25.39	26.82	28.18	30.00	31.57	32.81	33.98	34.64
1H-1, 27–28	0.27	7.53	7.65	8.29	9.27	10.63	12.24	13.84	15.71	18.15	19.57	20.05	20.96	22.02	23.77	25.45	26.77	28.18	29.96	31.45	32.62	33.87	34.44
1H-1, 37–38	0.37	7.94	8.07	8.74	9.82	11.20	12.99	14.82	16.91	19.18	20.63	21.36	22.26	23.38	25.29	26.96	28.46	29.87	31.71	33.26	34.48	35.74	36.47
1H-1, 47–48	0.47	8.62	8.79	9.54	10.73	12.37	14.39	16.50	18.69	21.21	22.68	23.30	24.36	25.49	27.47	29.34	30.92	32.48	34.42	36.09	37.36	38.83	39.58
1H-1, 57–58	0.57	8.97	9.11	9.91	11.12	12.83	14.94	17.06	19.34	21.73	23.56	24.19	25.15	26.28	28.27	30.17	31.70	33.24	35.06	36.74	38.05	39.50	40.30
1H-1, 67–68	0.67	9.57	9.76	10.61	11.90	13.66	15.85	18.08	20.39	23.02	24.44	25.09	26.07	27.17	29.18	31.13	32.72	34.25	36.19	37.86	39.14	40.67	41.48
1H-1, 77–78	0.77	9.12	9.24	9.99	11.23	12.79	14.81	16.87	18.93	21.49	22.73	23.31	24.21	25.31	27.26	29.01	30.61	32.17	34.03	35.72	37.10	38.47	39.33
1H-1, 87–88	0.87	8.70	8.80	9.52	10.66	12.22	14.16	16.03	18.09	20.53	22.13	22.51	23.50	24.53	26.53	28.24	29.76	31.22	33.13	34.81	36.09	37.54	38.38
1H-1, 95–96	0.95	8.31	8.42	9.10	10.25	11.74	13.63	15.65	17.77	20.15	21.30	21.87	22.77	23.79	25.64	27.32	28.94	30.47	32.25	33.91	35.13	36.44	37.20

Table AT1 (continued).

Core, section, interval (cm)	Depth (mbsf)	Wavelength (nm)																					
		470	480	490	500	510	520	530	540	550	560	570	580	590	600	610	620	630	640	650	660	670	680
188-1165B-																							
1H-1, 7–8	0.07	36.38	36.91	37.63	38.52	39.53	40.52	41.44	42.32	43.18	43.86	44.39	44.77	45.06	45.28	45.43	45.56	45.66	45.77	45.87	45.99	46.10	46.18
1H-1, 17–18	0.17	35.15	35.65	36.30	37.17	38.11	39.10	39.96	40.79	41.62	42.24	42.83	43.19	43.46	43.70	43.84	43.98	44.09	44.17	44.28	44.38	44.47	44.54
1H-1, 27–28	0.27	34.95	35.46	36.09	36.93	37.83	38.74	39.59	40.36	41.13	41.70	42.21	42.51	42.76	42.97	43.13	43.25	43.31	43.39	43.45	43.53	43.59	43.65
1H-1, 37–38	0.37	37.04	37.59	38.25	39.13	40.10	41.04	41.89	42.71	43.50	44.15	44.71	45.04	45.32	45.55	45.72	45.84	45.93	46.04	46.13	46.18	46.29	46.33
1H-1, 47–48	0.47	40.23	40.83	41.56	42.54	43.58	44.59	45.57	46.51	47.47	48.23	49.01	49.53	49.90	50.27	50.54	50.74	50.94	51.13	51.36	51.56	51.75	51.93
1H-1, 57–58	0.57	40.93	41.56	42.27	43.16	44.16	45.12	46.04	46.98	47.93	48.74	49.48	49.99	50.38	50.71	50.95	51.16	51.34	51.54	51.74	51.96	52.14	52.36
1H-1, 67–68	0.67	42.23	42.85	43.61	44.52	45.52	46.54	47.49	48.46	49.44	50.25	51.02	51.55	51.97	52.32	52.57	52.87	53.08	53.31	53.60	53.88	54.11	54.34
1H-1, 77–78	0.77	40.04	40.67	41.41	42.39	43.37	44.40	45.39	46.39	47.38	48.21	48.94	49.51	49.93	50.32	50.58	50.85	51.09	51.34	51.60	51.91	52.16	52.40
1H-1, 87–88	0.87	39.00	39.59	40.32	41.25	42.23	43.27	44.23	45.16	46.18	47.01	47.76	48.26	48.67	49.01	49.28	49.51	49.73	49.94	50.19	50.43	50.69	50.85
1H-1, 95–96	0.95	37.86	38.45	39.20	40.04	41.00	41.99	42.93	43.89	44.84	45.57	46.29	46.86	47.24	47.59	47.83	48.03	48.23	48.45	48.67	48.91	49.17	49.32

Table AT1 (continued).

Core, section, interval (cm)	Depth (mbsf)	Wavelength (nm)																
		690	700	710	720	730	740	750	760	770	780	790	800	810	820	830	840	850
188-1165B-																		
1H-1, 7–8	0.07	46.24	46.29	46.42	46.54	46.64	46.84	47.03	47.29	47.59	47.76	48.06	48.30	48.55	48.75	49.01	48.88	49.09
1H-1, 17–18	0.17	44.61	44.67	44.76	44.87	44.99	45.14	45.36	45.56	45.83	46.13	46.32	46.68	46.84	46.90	47.02	46.95	47.17
1H-1, 27–28	0.27	43.67	43.69	43.76	43.85	43.91	44.07	44.30	44.51	44.74	45.02	45.27	45.42	45.66	45.71	45.97	45.66	45.85
1H-1, 37–38	0.37	46.41	46.43	46.52	46.60	46.70	46.83	47.09	47.28	47.53	47.76	48.05	48.31	48.55	48.65	48.55	48.64	48.86
1H-1, 47–48	0.47	52.07	52.21	52.33	52.47	52.63	52.88	53.20	53.41	53.66	53.94	54.20	54.45	54.61	54.84	54.94	54.94	55.20
1H-1, 57–58	0.57	52.48	52.61	52.74	52.89	53.05	53.24	53.47	53.73	54.00	54.26	54.54	54.66	55.10	55.25	55.41	55.24	55.55
1H-1, 67–68	0.67	54.58	54.73	54.92	55.05	55.18	55.40	55.71	55.95	56.14	56.50	56.84	57.02	57.30	57.44	57.74	57.59	58.27
1H-1, 77–78	0.77	52.62	52.77	52.98	53.15	53.30	53.53	53.81	54.05	54.34	54.56	54.89	55.21	55.48	55.52	55.76	55.70	56.36
1H-1, 87–88	0.87	51.10	51.15	51.37	51.53	51.70	51.92	52.22	52.46	52.67	52.96	53.23	53.54	53.69	53.78	54.13	54.05	54.78
1H-1, 95–96	0.95	49.50	49.65	49.80	49.90	50.06	50.30	50.53	50.83	51.06	51.27	51.62	51.82	51.99	52.42	52.36	52.40	52.76

Notes: Samples were analyzed by PerkinElmer Lambda 6 instrumentation at the University of Texas at Arlington. Only a portion of this table appears here. The complete table is available in ASCII.